Journal of Volcanology and Geothermal Research 435 (2023) 107773

Contents lists available at ScienceDirect

Journal of Volcanology and Geothermal Research

journal homepage: www.journals.elsevier.com/journal-of-volcanology-and-geothermal-research

The propagation and emplacement mechanisms of the Tenteniguada volcanic debris avalanche (Gran Canaria): Field evidence for brittle fault-accommodated spreading

Symeon Makris [a,*], Matteo Roverato [b,c], Alejandro Lomoschitz [d], Paul Cole [a], Irene Manzella [a,e]

[a] School of Geography, Earth and Environmental Science, University of Plymouth, Plymouth, UK
[b] Department of Earth Sciences, University of Geneva, Switzerland
[c] Dipartimento di Scienze Biologiche, Geologiche e Ambientali, Alma Mater Studiorum, Università di Bologna, Italy
[d] Instituto de Oceanografía y Cambio Global, IOCAG, Universidad de Las Palmas de Gran Canaria, Las Palmas de Gran Canaria, Spain
[e] Department of Applied Earth Sciences, Faculty of Geo-Information Science and Earth Observation (ITC), University of Twente, Enschede, the Netherlands

ARTICLE INFO

Keywords:
Volcanic debris avalanche
Propagation processes
Facies
Canary Islands
Spreading
Gran Canaria

ABSTRACT

The Tenteniguada volcanic debris avalanche deposit is located on the east of the island of Gran Canaria, Spain. Its internal structure is composed of a complex assemblage of extensional features and shearing structures including normal faults, horst and graben, brittle/ductile boudinage and clastic dike injections. Examination of these features in the field and evaluation of their distribution have allowed the generation of a new conceptual model for the transport and emplacement of this debris avalanche, and potentially others. In the majority of the deposit, the degree of disaggregation is low, with large portions of the original edifice preserved, although displaced by brittle deformation. Greater disaggregation is observed deeper and in the more distal section of the deposit. The findings suggest that the propagation of the volcanic debris avalanche was most likely facilitated by the normal fault-accommodated spreading and extension of the mass, with the majority of stress focused in fault zones. The greater disaggregation exhibited in the deeper and the more distal part of the deposit is likely to be due to greater stress accommodation from fault convergence and momentum transfer respectively. The abundance of competent lava lithologies and scarcity of weaker material that could be easily disaggregated is the most likely reason Tenteniguada did not fully evolve from a slide to a granular flow, and therefore generated a deposit which bears resemblance to non-volcanic blockslide deposits. Therefore, lithological properties are potentially a vital factor for the propagation mechanisms, distribution of stress and consequently the evolution of a debris avalanche from the initial collapse to its emplacement. The present study highlights the importance of dedicated field examinations of sedimentological, morphological, and structural features for providing constraints for models of debris avalanche propagation mechanisms and the factors dictating them.

1. Introduction

Volcanic debris avalanches (VDA) are large landslide events generated by volcanic edifice flank collapses (Ui, 1983; Siebert, 1984; Shea and van Wyk de Vries, 2008; Roverato and Dufresne, 2021). Although the majority of VDAs occur on active volcanoes (Siebert, 1984; Voight, 2000), they are not necessarily triggered by volcanic activity, and can also be initiated by seismic activity or slope destabilisation due to precipitation, weakening or hydrothermal alteration of slopes composed of volcanic material (Belousov et al., 1999; Capra et al., 2002; Lomoschitz et al., 2008; Roverato et al., 2021). They are a common occurrence in the history of most volcanoes (Siebert and Roverato, 2021). Volcanic debris avalanche deposits (VDAD) mobilise volumes of up to tens of km^3, and less often up to hundreds of km^3. Due to their high volumes and mobility, VDAs pose a significant hazard to communities close to volcanoes.

The runout of VDAs is greater than what is predicted by simple frictional models of a solid block (Legros, 2002). The coefficient of friction, measured as the H/L ratio between the elevation loss (H) and runout in the direction of flow (L), has been used as a measure of VDA mobility and rock avalanches (RAs), the equivalent process in non-volcanic settings (e.g. Heim, 1932; Shreve, 1968; Erismann, 1979;

* Corresponding author.
E-mail address: symeon.makris@plymouth.ac.uk (S. Makris).

https://doi.org/10.1016/j.jvolgeores.2023.107773
Received 23 September 2022; Received in revised form 11 February 2023; Accepted 14 February 2023
Available online 21 February 2023

Hürlimann and Ledesma, 2003). Although simple frictional models would predict H/L values of ~0.5–0.6, VDAs typically achieve values of 0.1–0.2 (Legros, 2002; Dufresne et al., 2010a, 2021a). While many theories have been proposed to explain the mechanisms that enable this runout, the issue remains controversial and unresolved (Banton et al., 2009; Davies and McSaveney, 2012).

The difficulty of models and theoretical concepts to constrain VDAD field observations of sedimentology and structure is a major factor for the lack of explanation (Johnson et al., 2014; Perinotto et al., 2015). VDADs exhibit a set of typical features, such as jigsaw-fractured clasts, block and matrix-rich facies, remnant stratigraphy, textural and sedimentological heterogeneity and hummocky surfaces (Siebert, 1984; Glicken, 1991; Roverato et al., 2015; Makris et al., 2020; Dufresne et al., 2021b). However, the variability they exhibit in facies and sedimentological composition, internal structure and longitudinal evolution are unattained by a single conceptual, analogue or numerical model. This results from the lack of understanding of VDA/RA propagation mechanisms and the factors dictating their dynamics according to material properties and other parameters. For example, theories which propose a plug flow over an agitated basal layer, such as suggested by Campbell (1989) and Takarada et al. (1999), find support in deposits such as Iwasegawa and Kaida VDADs (Takarada et al., 1999) which preserve such a basal layer. However, the observation of sheared material in the body of landslides such as the Pungarehu VDAD, Taranaki volcano, New Zealand (Roverato et al., 2015), Tschirgant RA, Tyrol, Austria (Dufresne and Dunning, 2017) and the deposit examined by the current study indicates that a hypothesis based entirely on stresses accommodated in a basal layer cannot be the primary explanation for the mobility of all VDAs/RAs, as also suggested by Johnson et al. (2014). Therefore, more dedicated field studies are required, in order to define constraints for the development of models regarding the kinematics and dynamics of VDA/RA propagation and emplacement which are consistent with the morphology and structure of their deposits (Cruden and Varnes, 1996; Pudasaini and Hutter, 2007; Shea and van Wyk de Vries, 2008). Propagation encompasses the initial collapse and acceleration of the mass, while emplacement refers to the final deceleration and ultimate deposition of the material (Paguican et al., 2021). In line with this, recent work has highlighted the importance of dedicated field studies to better identify structural and sedimentological features such as facies and feature distribution in order to evaluate VDA/RA dynamics (including but not limited to Smyth, 1991; Glicken, 1996; Roverato and Capra, 2013; Roverato et al., 2015; Dufresne et al., 2016; Dufresne and Dunning, 2017). Such studies allow the reconstruction of pre- and *syn*-propagation and emplacement history (Dufresne et al., 2010b). Thus, they bridge the gap between models and theoretical concepts and field observations of sedimentology and the structure of deposits, identify the factors leading to these processes and provide constraints for the propagation mechanisms (Perinotto et al., 2015).

The present study examines the deposit of the Tenteniguada VDA (Ten-VDA), located on the east of the island of Gran Canaria, Spain (Fig. 1). This well-preserved and exposed deposit presents an opportunity to study internal structures and their distribution and sedimentology. The aim of this study is to evaluate the Ten-VDA propagation and emplacement processes and the factors that controlled its material behaviour, stress accommodation and deformation history. The deposit is initially described by its structural and sedimentological features and specific outcrop properties. Their implications for the dynamics of the Ten-VDA are subsequently discussed, also in association to other deposits and theoretical and numerical models. The structural features of the Ten-VDAD and their evolution offer an insight into the dynamics of VDAs as they evolve from a slide of the initial edifice portion to a fluidised flow. Findings are relevant to VDAs composed of competent non-granular material, as well as other mass movements, such as rockslides, with the potential of further constraining their behaviour in conceptual models, and contributing to the assessment of related hazards.

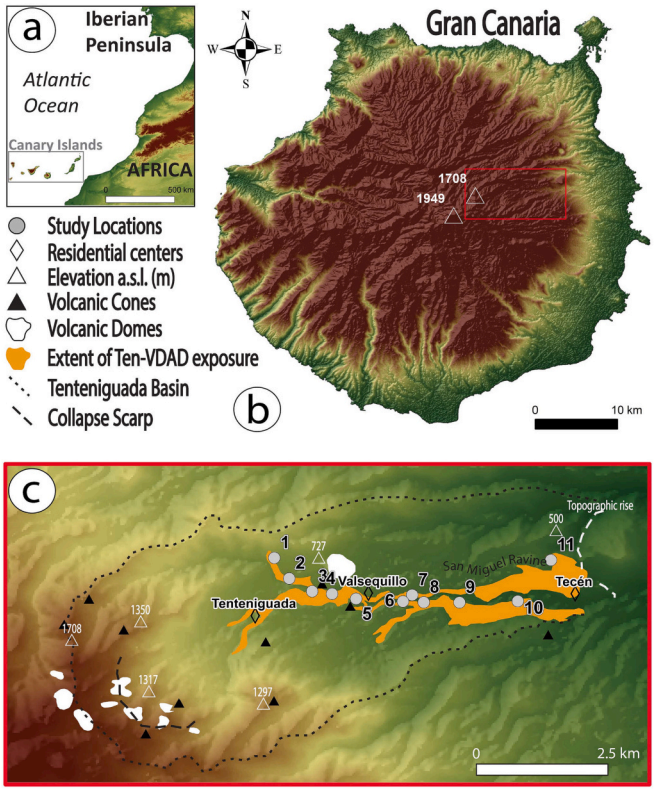

Fig. 1. a Location of the Canary Islands. b The Island of Gran Canaria with the location of the Tenteniguada basin (red rectangle – also indicates the extent of c). c The Tenteniguada debris avalanche deposit is exposed on the walls of the San Miguel Ravine in the Tenteniguada basin due to fluvial incision. (For interpretation of the references to colour in this figure legend, the reader is referred to the web version of this article.)

2. Geological and regional background

2.1. Geological background

All volcanic products on the island of Gran Canaria have been formed in the last 15 Ma (Lomoschitz et al., 2008). According to Funck and Schmincke (1998), this has taken place in three major magmatic cycles during the evolution of the Roque Nublo volcanic edifice, a classic stratovolcano formed in the collapsed proto-volcano Tejeda Caldera:

1. Rapid growth of a basaltic shield volcano in the Miocene was followed by the collapse of its centre to form the Tejeda Caldera. Subsequently, a 500–1000 m thick sequence of ignimbrites, lava flows and intrusive volcanics was formed in an eruptive phase. Finally, in the Miocene, the volcano experienced a volcanic activity hiatus of 3–4 Ma.
2. In the Pliocene, the Roque Nublo edifice >1000 m in height was constructed over the Miocene caldera. This period is represented in deposits of lava, pyroclastic flows, lahars, VDAs and intrusive phonolite domes.
3. Quaternary volcanism was limited to the northeast half of the island. This period is characterised by basanite lavas, pyroclastics and volcanic cones.

The Roque Nublo edifice was a classic stratovolcano consisted of alternating lava flows and pumiceous ignimbrites as well as lahars, conglomerates, and debris flow deposits (Mehl and Schmincke, 1999). Its cone at the centre of the island reached at least 2500 m tall ~3 Ma ago. However, the steep slopes made the structure unstable and at the time of the Ten-VDA gravitational collapses produced a horse-shoe

amphitheatre open to the south and reduced the edifice height (Perez-Torrado et al., 1995). The most important collapses were in the south-southwest sector of the island (Lomoschitz et al., 2008) therefore some slopes might have been more prone to collapse in the east, where the Ten-VDA occurred.

The Ten-VDAD overlies Mio-Pliocene rocks, and is overlain by Plio-Quaternary volcanic and sedimentary lithologies. Therefore, it is related to the second and third stages of the Roque Nublo development. Although its age is still not well constrained, Lomoschitz et al. (2008) place it between 276 ka and 1.97 Ma, in the Lower-Middle Pleistocene. From this phase, several VDAs have distributed material from the central highland towards the coastline (Mehl and Schmincke, 1999). The well-preserved hummocky paleotopography displayed at the top of the Ten-VDA deposit suggests an age close to the age of the overlying basanite lava flows, i.e. ca. 276 ka. The lack of *syn*-eruptive pyroclastic deposits suggests that the triggering of the Ten-VDA was not related to a volcanic eruption according to the findings of Lomoschitz et al. (2008). Instead, Lomoschitz et al. (2008) suggest that it could have been triggered by a proximal earthquake unrelated to volcanic activity on Gran Canaria. The basanite lava flows that overly the deposit have contributed to the preservation of the deposit and protection from erosion.

2.2. Paleoclimate

The paleoclimate of the eastern Canary Islands during the Pleistocene has been assessed through the marine fauna in fossiliferous deposits by Meco et al. (2002, 2003). During the Miocene the climate was tropical, with low variability. However, ~3 Ma ago the climate became dominated by alternate humid and arid episodes. In the Quaternary, humid episodes enabled significant geomorphic disturbance in the area and have potentially had the effect of incising the paleoravine in which the avalanche propagated, conditioning the slope for the collapse of the Ten-VDA by raising the water table (Lomoschitz et al., 2008). One of these humid episodes (potentially ~420 ka ago) is suggested by Lomoschitz et al. (2008) to have contributed to the destabilisation of the mass, leading to the collapse of material that evolved to the Ten-VDA.

2.3. Edifice and deposit morphology

The Ten-VDAD is exposed along the San Miguel ravine, in the eastern part of the island of Gran Canaria (Fig. 1). The VDA was, at least partially, channelized by a paleoravine at the same location and is exposed along the walls of the modern ravine by fluvial incision. Initially described by Balcells et al. (1990) as a Pliocene gravitational, non-volcanic landslide, it was later reported as a Quaternary VDA by Quintana and Lomoschitz (2005) and described in greater detail by Lomoschitz et al. (2008). The San Miguel Ravine has an area of 22.5 km^2 and a semi-circular head scarp crowned by phonolite domes (Fig. 1) (Lomoschitz et al., 2008). The current head of the valley has a maximum elevation of 1708 m a.s.l.

The runout of the Ten-VDA was ~8.5 km, with an average width of 1.5 km and a deposit length of 7.1 km (Lomoschitz et al., 2008). The slope of the valley floor during the Ten-VDA was ~22° (Lomoschitz et al., 2008). Although the Ten-VDA was relatively small, with a deposit volume of 0.35 km^3, it still achieved an H/L ratio of ~0.16. This is comparable to other VDAs and is significantly lower than the 0.5–0.6 predicted by simple frictional models (Davies, 1982; Ui, 1983; Legros, 2002). The thickness of the exposed outcrops of the deposit is variable between <5 m and > 50 m, although the base of the deposit is not exposed, and therefore the true thickness could not be evaluated. The deposit terminates at a topographic rise (Fig. 1c), which could have aided the termination of the propagation of the Ten-VDA (Lomoschitz et al., 2008).

3. Composition and internal structure of the Ten-VDAD

The exposed and accessible outcrops of the deposit, which were examined for this study, are illustrated in Fig. 1 (and the table describing the outcrops in complementary material Appendix A). Field observations suggest that the deposit is dominantly composed of Pliocene phonolite–ignimbrite and basalt to tephrite lavas. These lithologies behave as the more competent, undisaggregated material in the Ten-VDAD. The basalt-tephrite is the most competent, often preserved as massive, homogenous VDA blocks (e.g. Fig. 2). The phonolite-ignimbrite is less competent and more frequently suffers greater fragmentation generating a higher proportion of matrix (Lomoschitz et al., 2008). All the above-mentioned lithologies preserve the characteristic jigsaw-fractured pattern of VDA blocks (e.g. Fig. 3a) (e.g. Siebert, 1984; Glicken, 1991). Jigsaw-fractured blocks and clasts exhibit a chaotic fracture network, where *syn*-propagation-generated fragments experience little relative displacement resulting in the lack of disaggregation of the fractured rock unit as illustrated in Fig. 2c and 3a (e.g. Ui, 1983; Glicken, 1996; Bernard et al., 2021). Fragmented clasts remain coherent without dispersion of their components despite the fractured structure imposed on them (Pollet and Schneider, 2004). Therefore, a jigsaw-fit fabric of dense fracturing but no disaggregation and displacement of the component angular clasts is imposed on the material.

The deposit also contains a small proportion of hydromagmatic, and pyroclastic material (Lomoschitz et al., 2008). This material is weaker and generates cataclased disaggregated blocks which do not preserve jigsaw fracturing. There is no evidence of hydrothermal alteration of the material prior to the Ten-VDA. Horizons with a distinctive red colour mark lithological boundaries within the body of the Ten-VDAD (Fig. 4). These are baked margins likely generated by temperature increase of material underlying lava flows in the stratigraphy of the material composing the volcanic edifice. Baked margins also consistently mark the top of the Ten-VDAD and its contact with the overlying basanite lava flow, which is exposed in the majority of the outcrops. These horizons are the result of a younger, overlying basanite lava flow increasing the temperature of the top of the deposit and generating the colour change of its upper boundary.

With the base of the deposit not exposed, substrate incorporation is only evident by a ripped-up block at location 6, which is the only one observed. The block is surrounded by the mixed facies to which it has been incorporated when detached from the substrate (Fig. 5a). The sedimentation of sand lenses near the top of the block (Fig. 5a) and pumice-rich horizons at its base (Fig. 5b) are likely to be related with water flow. Therefore, the material has been interpreted as a secondary deposit, incorporated from the path of the propagating avalanche. A set of normal faults displace the strata at the base of the block (Fig. 5b).

3.1. Facies composition and distribution

The deposit can be subdivided into the characteristic volcanic debris avalanche facies: the matrix-rich facies (after Roverato et al., 2011; matrix/mixed facies in previous VDA literature after Glicken, 1991) and the block facies (after Ui, 1989; Glicken, 1991). The term matrix is used in the sedimentological sense of finer grains surrounding larger particles (Mehl and Schmincke, 1999), which is scale-dependent rather than assigning a particular size (Vezzoli et al., 2017).

3.1.1. Block facies

The Ten-VDAD is composed of a large proportion of blocks of the original volcanic edifice that are undisaggregated as exemplified in Fig. 2, having suffered little fracturing, and in some cases preserving original stratigraphic sequence (Figs. 4, 6). The term block is here used to refer to an unconsolidated, or poorly consolidated, portion of the source edifice transported and emplaced by the Ten-VDA, remaining unmixed with outside material (Glicken, 1991; Bernard et al., 2021). Fracturing refers to the fragmentation of a block resulting in a fabric of

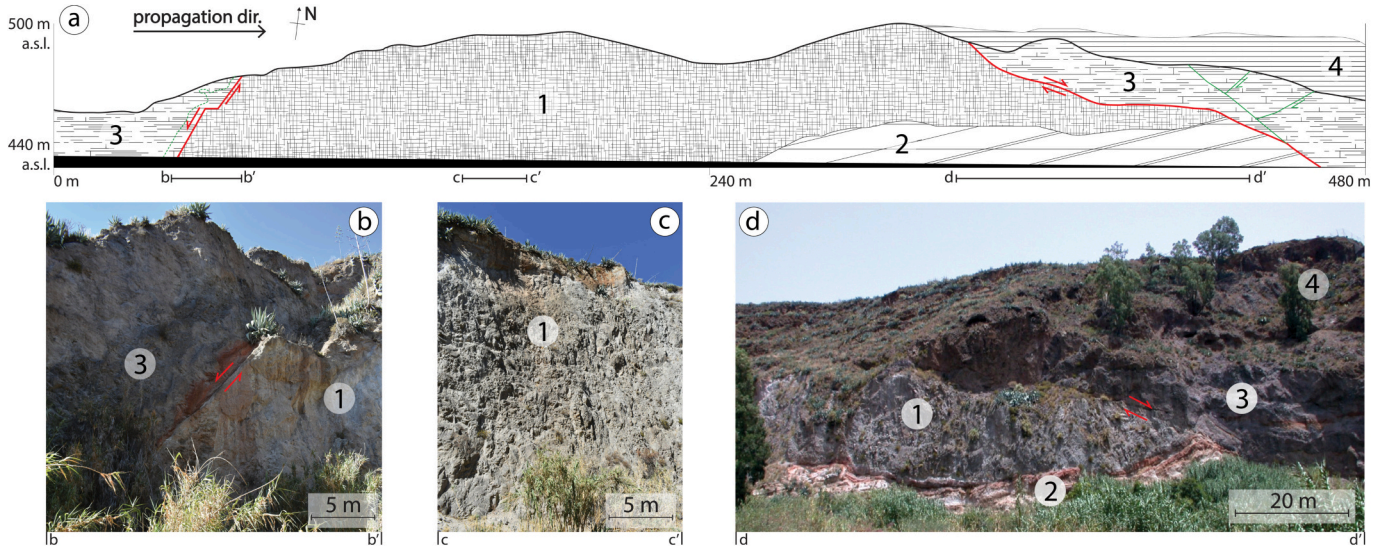

Fig. 2. Location 7 represents a horst and graben structure with the largest exposed block of the deposit and normal faults on either side. a Schematic representation of the outcrop. b Proximal-facing normal fault and adjacent block to the west of the central block. c Central block with jigsaw-fractured undisaggregated fabric. d Distal-facing normal fault and adjacent block to the east of the central block. Legend 1. Jigsaw-fractured tephrite lava. 2. Ash and pumice phonolite deposit (1 and 2 are part of the same block, transported together). 3. Jigsaw-fractured tephrite lava (distinct lithology to 1). 4. Younger basanite lava flows over the Ten-VDAD.

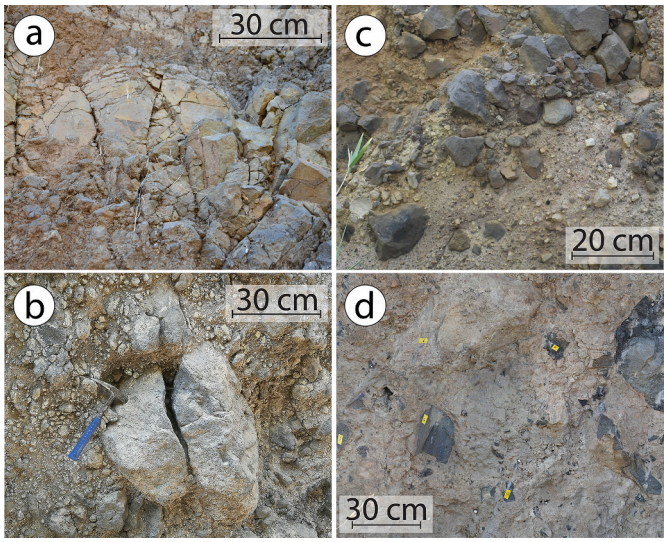

Fig. 3. Progressive disaggregation of material from jigsaw-fractured clast (a) to interblock/intrablock matrix (d). The evolution is illustrated through clasts at different stages of disaggregation. a Jigsaw-fractured clast with component fragments preserving their original position. b Widening of the gap between clast components has provided space for the finer particles in the matrix to intrude. The outline of the original clast has been deformed. c Components of the original clast have diffused and the original outline of the clast has been eliminated. Incomplete mixing is evident by the concentration of clasts of identical lithology in a more heterolithic matrix. d A completely mixed, poorly sorted homogenous assemblage of clasts and matrix where clasts have been incorporated in and mixed with the matrix and no jigsaw fracturing is preserved.

individual clasts composing it. Disaggregation implies the displacement of these components within a block, distorting the original placement, structure and outline (Fig. 3). Blocks in the Ten-VDAD consist of relatively coherent blocks of phonolite, tephrite and to a lesser extent pyroclastic material (Lomoschitz et al., 2008). Conversely, fine material and matrix represent a very minor proportion of the deposit. Blocks reach tens of metres in exposure (Fig. 2). The majority of blocks that preserve their original stratigraphy exhibit back-tilting compared to their original orientation as illustrated in Figs. 4 and 6.

Blocks which preserve their original stratigraphy and texture that have not been jigsaw-fractured or disaggregated are exhibited at locations 2 (Fig. 6), 4 (Fig. 4), and 7 (Fig. 2). Such blocks do not include any fine matrix. They are exclusively encountered higher up in the exposures, shallower in the deposit, and not close to the modern ravine floor. Moreover, blocks with a jigsaw-fractured texture occur from the most proximal location 2 and up to location 8 (Fig. 2c, 3a, 4). Such blocks exhibit a jigsaw-fit fabric composed of angular clasts. Nonetheless, clasts are not displaced relative to each other, and therefore the blocks remain fractured but undisaggregated (Fig. 7a). The majority of such blocks correspond to basalt and tephrite lava flows which are massive and homogenous (Lomoschitz et al., 2008). The largest such block observed in the Ten-VDA, in location 7, is >300 m in width and > 50 m high (Fig. 2c). The block is composed of jigsaw-fractured tephrite lava, which has not been disaggregated and contains very little fine material and no matrix.

Other blocks are more severely fractured, cataclased and brecciated, nonetheless preserving their lithlogical distinctness and external boundaries unmixed (Fig. 7b-d). Cataclasis refers to the gradual fracturing, comminution, disaggregation and production of matrix that generates in such blocks the diamicton fabric illustrated in Fig. 7d. These cataclased blocks are most frequently exhibited in the distal areas of the deposit after location 7, but also lower in the exposures of the more proximal locations 2, 4, 5, 7 and 8. In these cases, a chaotic mixture of subangular to subrounded clasts is surrounded by a fine matrix of the same lithology, producing the diamicton texture (Fig. 7c, d). This intrablock matrix (terminology after Roverato et al., 2015) exhibits greater mixing and poor sorting of more comminuted clasts composed of the same material represented in the blocks. In the Ten-VDAD the intrablock matrix is in most cases silty to sandy in grain size and its proportion of the total volume is variable in different blocks according to the degree of cataclasis. The intrablock matrix is composed of one or more lithologies represented in the block. For example, the exposure at location 10 is composed of a monolithological disaggregated lava that has been fractured and evolved to a matrix-supported mixture of poorly sorted subangular clasts in an intrablock matrix of identical lithology (Fig. 7c).

Diffuse contacts between blocks and the intrablock matrix as well as

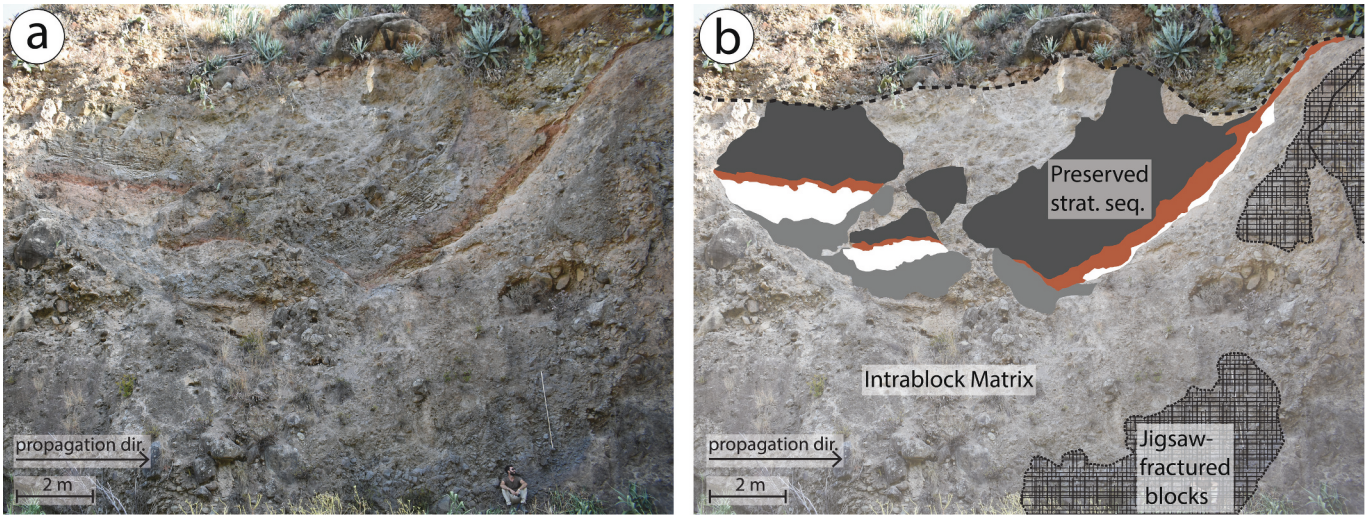

Fig. 4. The outcrop in location 4 is composed of a block with components of variable disaggregation. It exhibits a component of preserved stratigraphy higher up in the outcrop, and jigsaw-fractured undisaggregated components lower down. The rest of the block is composed of an intrablock matrix. a Red horizons illustrate stratigraphic preservation (red shaded area in b). Person for scale. b Annotated image of the same outcrop. The dashed line marks the top of the deposit. The shaded areas represent distinct lithological units, illustrating the preserved stratigraphy. (For interpretation of the references to colour in this figure legend, the reader is referred to the web version of this article.)

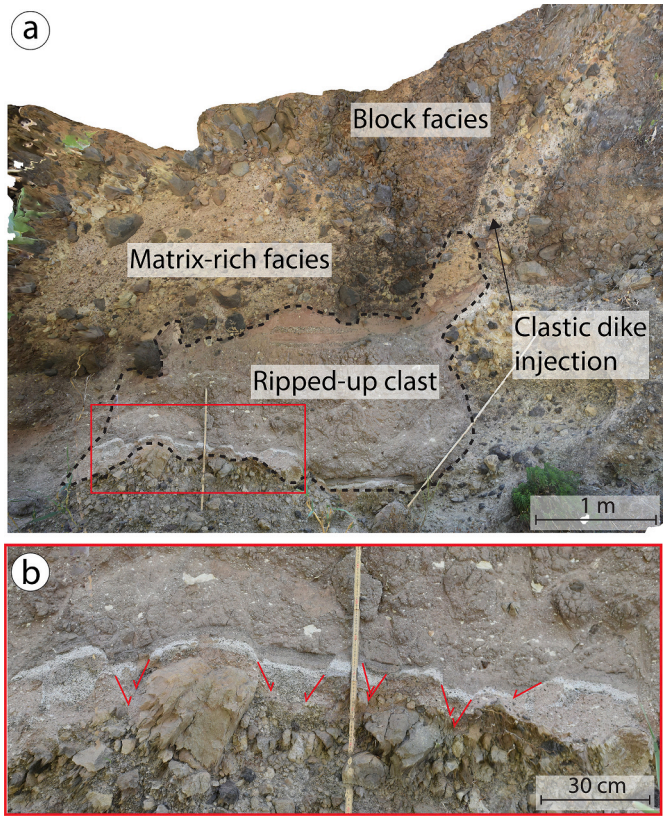

Fig. 5. a At location 6 the deposit exhibits matrix-rich facies, block facies, and a block that has been incorporated from the substrate. The matrix has been injected as a clastic dike in the block facies. Red rectangle represents the extent of b. b At the base of the ripped-up block a series of normal faults have been generated, marked by the red lines. (For interpretation of the references to colour in this figure legend, the reader is referred to the web version of this article.)

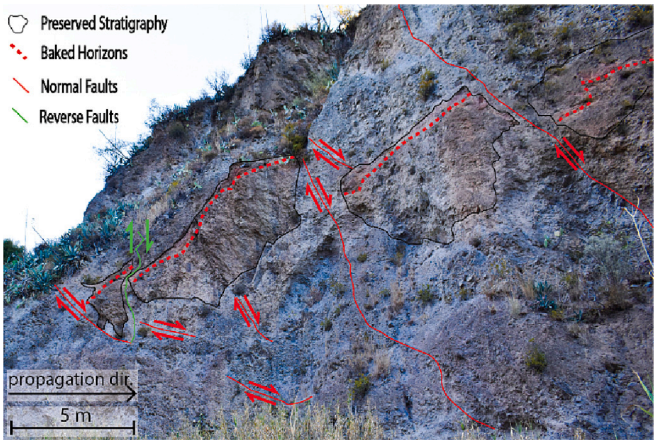

Fig. 6. Part of the outcrop at location 2. Back-tilted blocks displaced to each other by normal faults have adopted a brittle shearband boudinage form. The blocks preserve their original stratigraphy (observable by the continuity of the red baked layers indicated by the red dashed line). More cataclased blocks of lava lithologies are exposed in the rest of the outcrop. (For interpretation of the references to colour in this figure legend, the reader is referred to the web version of this article.)

blocks and the matrix-rich facies have been observed, although not a common feature in the deposit (Fig. 8). In such block boundaries, the particles composing the undisaggregated component of a block diffuse outwards mixing with the matrix surrounding them. In the periphery of the block, gaps are created between the particles which diffuse outwards. These gaps are intruded by outside material. These features illustrate local gradual mixing. Such contacts have only been observed in the lower sections of the exposures, closer to the valley floor. Except for the jigsaw fractures and signs of incomplete mixing in the matrix, there are no other intrablock structures.

3.1.2. *Matrix-rich facies*

The matrix-rich facies is exhibited from the more proximal locations 3, 5 and 6 to the most distal location 11 composed of a very poorly sorted, matrix-supported mixture of clasts and a fine interblock matrix (Fig. 9). However, it only constitutes a small proportion of the deposit.

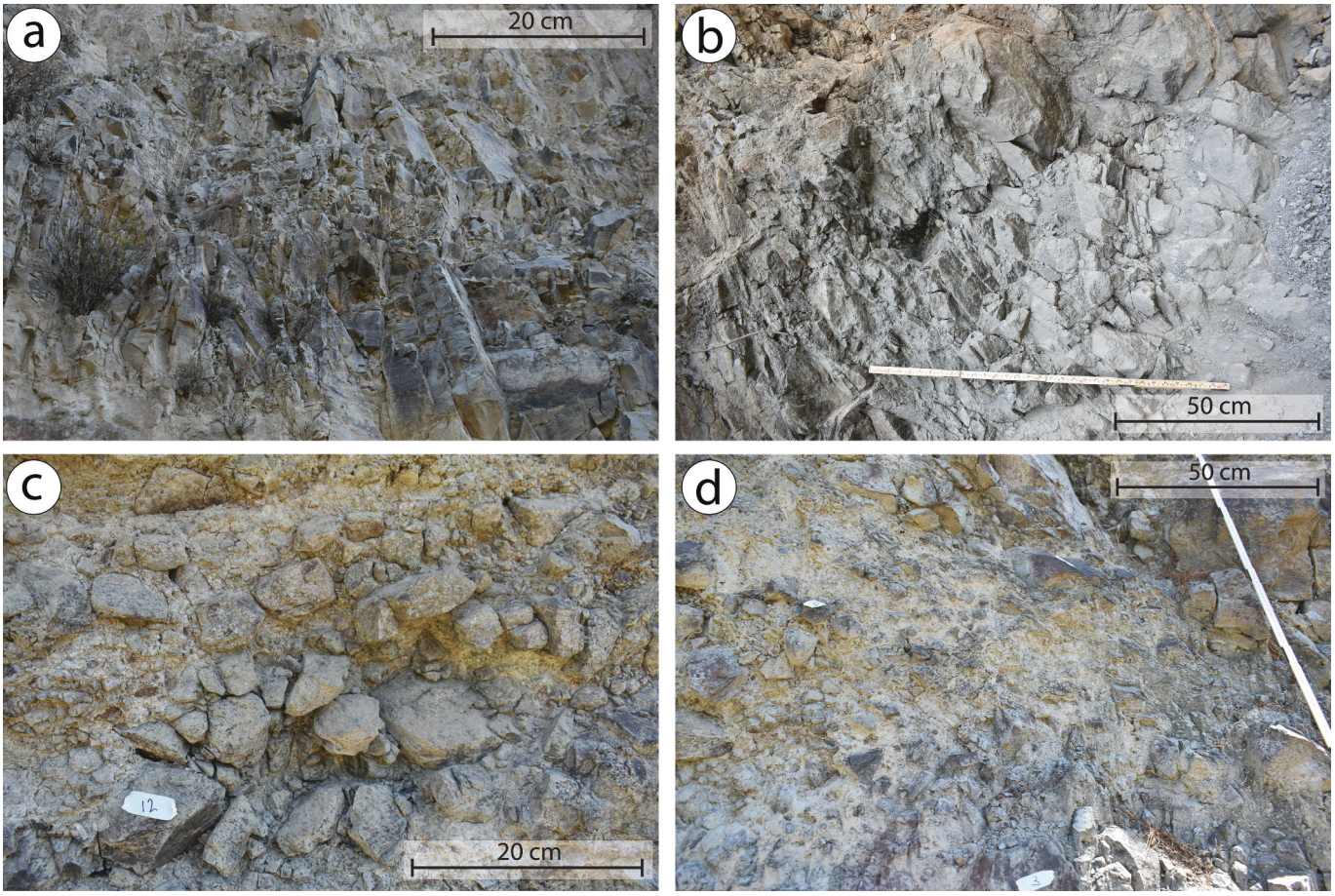

Fig. 7. Stages of disaggregation from jigsaw-fractured block to monolithological diamicton illustrated through blocks at different stages of disaggregation. a Undisaggregated jigsaw-fractured block where the components are not displaced (location 2). b In this block angular clasts composing the jigsaw-fit fabric preserve their original order, however, small quantity of fine material has been generated between them (location 9). c The original structure of the component clasts has been eliminated and the block has the fabric of a monolithologic breccia (location 10). d The block here exhibits the texture of a matrix enriched, disaggregated, matrix-supported monolithological diamicton (location 2).

Particles in the matrix-rich facies vary in size from micrometres, in the matrix, up to clasts >50 cm (e.g. Fig. 9). Both components comprise lava flow lithologies as well as the hydromagmatic and pyroclastic fall layers of phonolitic composition that are originally less consolidated, with a granular texture. Such material in the initial collapsed edifice transition into the matrix-rich facies more easily (Lomoschitz et al., 2008). Clasts are angular to subrounded and are, on average, more rounded than the component clasts of jigsaw-fractured blocks. The term matrix-rich (Roverato et al., 2011) is used instead of mixed because the material is not always completely mixed (completely mixed material illustrated in Fig. 3d, 9c) as defined by Glicken (1991). The facies forms a hetero-lithological, poorly sorted mixture of clasts and matrix. Nonetheless, incomplete mixing is evident by the components of fractured blocks that have been deposited in the process of relative displacement and diffusing into the matrix as is illustrated by Fig. 9a, b. At block boundaries, where cataclased blocks are being mixed with the matrix, their boundaries are incorporated into the matrix in diffuse margins (Fig. 8a, b).

3.2. Brittle features

Normal faults are exhibited at different scales in the deposit, and they are very common from the most proximal section of the deposit until location 8 (Figs. 2, 10). The majority of the faults are not continuous to the base of the deposit and change directions and merge lower. This is evidence that they are *syn*-propagational and not post-emplacement features. In location 7, illustrated in Fig. 2, a large tephrite block (Fig. 2c) is in contact with more fractured darker tephrite lava blocks on both sides (Fig. 2b, d) of the exposure (Lomoschitz et al., 2008). The back-tilting generates a toreva block feature. The contact represents normal faults on either side of the block, one proximal-facing and one distal-facing (Fig. 2a), constituting the large block as a horst feature, which could have formed a hummock on the surface of the deposit.

At a smaller scale, normal faults are exhibited in the block facies displacing components of blocks (Fig. 10) accommodated by normal faults. Additionally, blocks composed of portions of the original edifice of identical preserved stratigraphic sequence are exhibited displaced in relation to each other and tilted back towards the source of the Ten-VDA, without exhibiting a discrete fault plane. Such blocks are exposed, for example, in locations 4 (Fig. 4) and 2 (Fig. 6). In location 2, the displacement between blocks has been accommodated in a brittle-ductile manner by surrounding intrablock matrix, giving the modules of the original block a brittle shearband (Goscombe et al., 2004) boudinage form (Fig. 6). The deformation was accommodate by the intrablock matrix and blocks were displaced while not deformed. The resulting form is of asymmetric brittle shear/domino boudins displacing and back-tilting the components of the initial single block. This brittle behaviour is most abundant higher in the outcrops, although a few examples of brittle behaviour were encountered close to the modern ravine floor. These features are limited to the block facies.

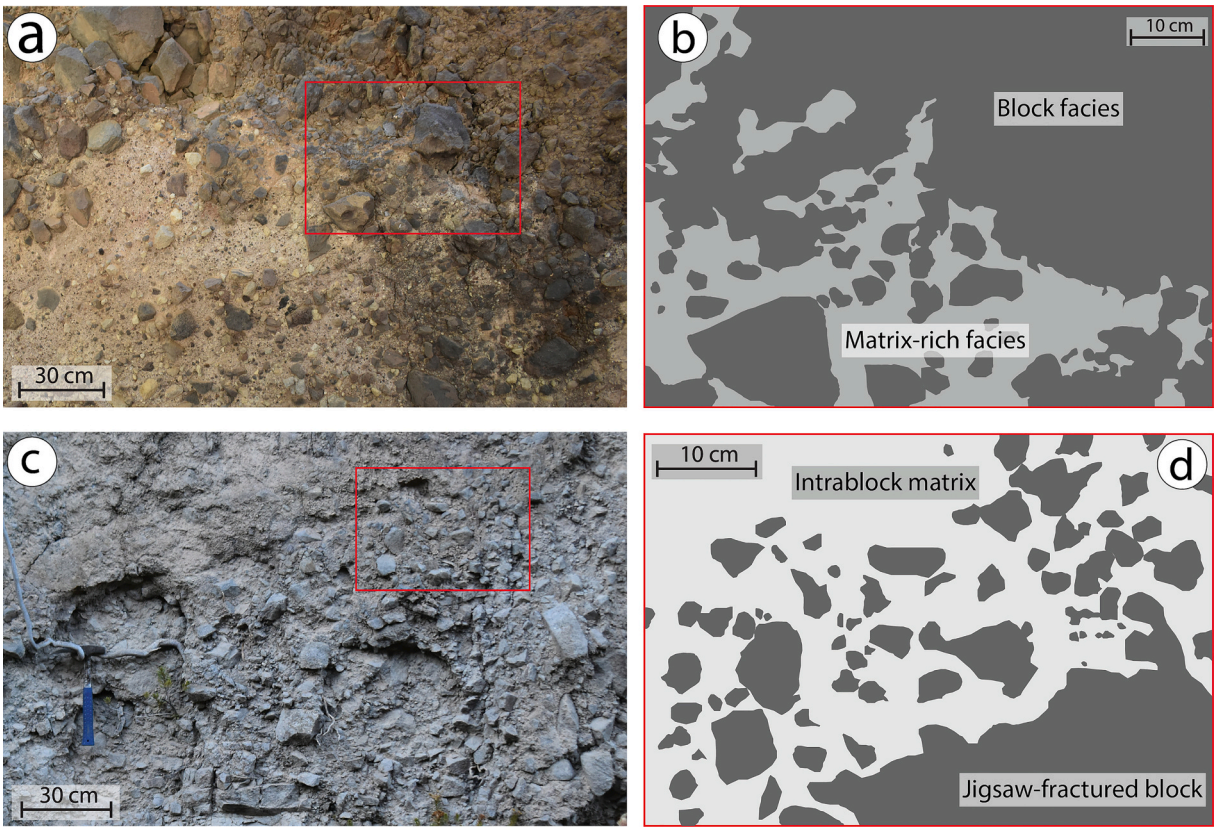

Fig. 8. Diffuse contacts between the block facies and the matrix-rich facies (a, b) and between undisaggregated material and intrablock matrix within the matrix-rich facies (c, d). The red rectangles in a and c, represent the extent of b and d respectively. Material from the margins of undisaggregated blocks is exhibited diffusing and being incorporated into the matrix. (For interpretation of the references to colour in this figure legend, the reader is referred to the web version of this article.)

3.3. Shearing and fluidal features

Shearing is illustrated by components of fractured clasts displaced in parallel, but opposite directions (Fig. 11a). Sheared clasts are exhibited in the matrix-rich facies and highly disaggregated blocks in the block facies. However, they do not occur in the interior of blocks that are less disaggregated and preserve jigsaw fractures. Sheared material is exhibited lower in the exposures, and not higher on the ravine walls where stratigraphic preservation is more frequent.

However, shearing and fluidal behaviour is also observed at the boundaries between blocks. A shearband boudinage (Goscombe et al., 2004) feature is illustrated in Fig. 11b between blocks. A flame injection of a clastic dike is exhibited in the normal fault between two blocks in location 7, suggesting shear between the blocks when the fault was active (Fig. 11c-d, 2b). In location 6, illustrated in Fig. 5, a clastic dyke injection of matrix-rich facies between blocks offers evidence of fluidal behaviour lower in the deposit. Other than these limited specific circumstances, in the interior of both the block and the matrix-rich facies, there is no evidence of mass shearing.

3.4. Longitudinal evolution

The deposit can be longitudinally separated into two distinct sections according to the internal structure and degree of disaggregation of the material: 1. Block facies with relatively low disaggregation, with blocks that preserve their jigsaw-fractured texture, compose the majority of the volume of the proximal exposures, and up to location 8. 2. Block facies at the more distal locations 9 and 10 (as well as exposures between them), do not preserve a jigsaw-fractured texture, except in few cataclased blocks that remain fractured but undisaggregated within the intrablock matrix. Blocks are more disaggregated and cataclased with component clasts displaced in relation to each other. In these blocks, the proportion of interblock matrix is greater. The degree of cataclasis and disaggregation generated the fabric of a monolithological diamicton (Fig. 7c-d). Normal faults and brittle behaviour as well as shearing features are not observed in this distal section. Clasts in more disaggregated blocks are subangular to subrounded (e.g. Fig. 7c-d); more rounded than the angular to subangular clasts in jigsaw-fractured blocks (e.g. Fig. 7a-c). Nonetheless, the unmixed lithological distinctness of blocks is preserved.

4. Discussion

4.1. Brittle extensional behaviour

Extensional normal faults, horst formation and boudinage indicate the accommodation of extension during propagation. Normal fault alignment perpendicular to the propagation direction offers an indication of the extensional regime (Longchamp et al., 2016; Roberti et al., 2017). Such normal faults have been also observed in other VDADs (e.g. Siebe et al., 1992; Glicken, 1996; Siebert et al., 2006; Bernard et al., 2008; Roberti et al., 2017), with the Socompa VDAD being an illustrative example (Longchamp et al., 2016). Similar horst and graben structures are also reported in the Delcamp et al. (2017) study of the Momella VDAD. In the Ten-VDAD blocks of identical stratigraphy have been fractured and separated into smaller modules, subsequently displaced and back-tilted, as illustrated in Figs. 4 and 6. Further evidence for the extension is offered by the lack of vertical stratigraphic repetition in all the faults, supporting the lack of extensive compressional environments as supported by Shea and van Wyk de Vries (2008). It is also probable that the lateral confinement of the avalanche by the ravine and frontal by the topographic rise at its toe generated compressional

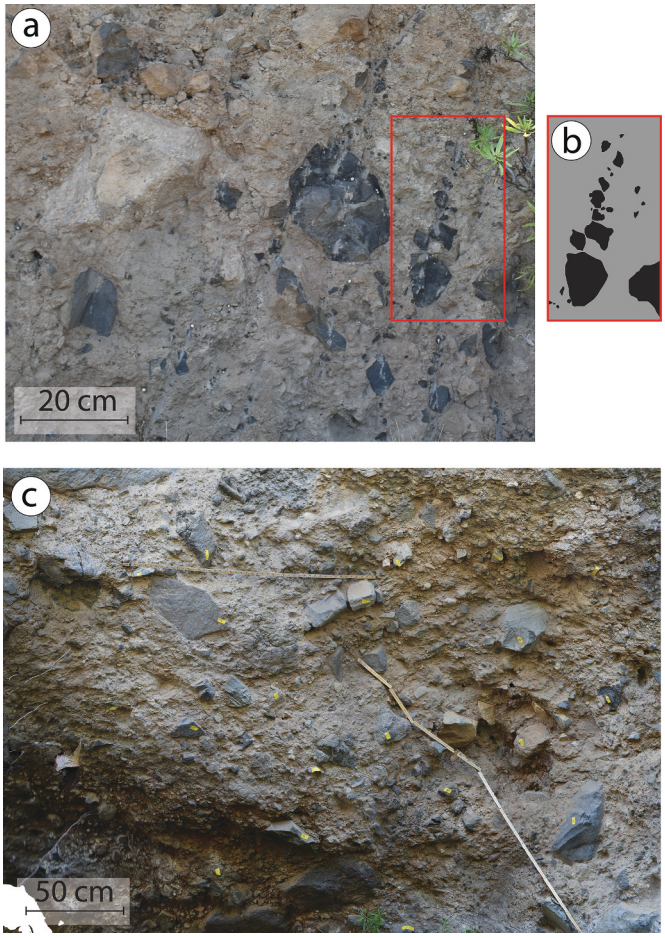

Fig. 9. Matrix rich facies. a The poorly sorted heterolithological matrix rich facies exposure at location 11. The red rectangle represents the extent of b. b Incomplete gradual mixing is illustrated by clasts of identical origin preserved while diffusing into the matrix. c Mixed, poorly sorted mixture of clasts and matrix with no internal features in the matrix-rich facies in location 3. (For interpretation of the references to colour in this figure legend, the reader is referred to the web version of this article.)

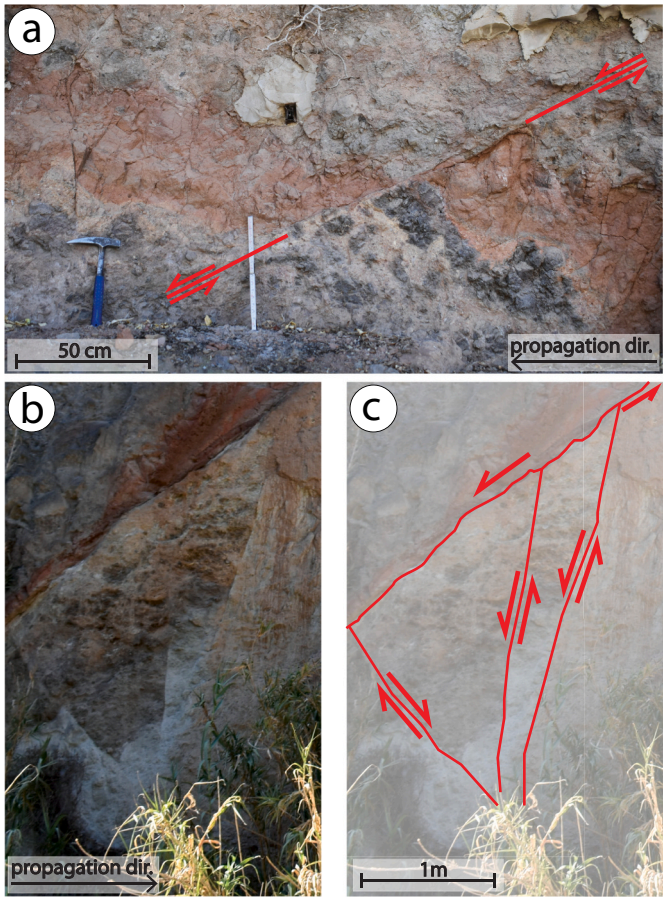

Fig. 10. Small-scale normal faults. a Red baked horizon illustrates the normal fault at location 8. b Section from location 7. c. Section from b with normal faults annotated. (For interpretation of the references to colour in this figure legend, the reader is referred to the web version of this article.)

regimes and features in these areas. However, representative outcrops are not exposed. The small number of reverse faults, of limited extent (e.g. Figs. 4, 6), potentially reflect momentum transfer in the material during propagation, as is later discussed. The abundance of brittle features observed in the majority of the deposit suggests large-scale brittle-type behaviour as the principal mode of propagation of the Ten-VDA (Shea and van Wyk de Vries, 2008; van Wyk de Vries and Delcamp, 2015). Shear was concentrated at the normal faults, as also suggested for the Momella VDAD by Delcamp et al. (2017). Focusing of shear stress at fault zones allowed the low degree of disaggregation and fragmentation at the interior of blocks. This results in the low amount of fine material and matrix generated, low disaggregation and a high degree of preservation, constituting a deposit that more closely resembles a non-volcanic blockslide deposit than a typical VDAD, as also observed in the case of the Jocotitlán VDAD by Dufresne et al. (2010b). The lack of fine, loosely consolidated, weak or hydrothermally altered material in the original destabilised portion of the edifice is likely to have contributed to this aspect of the character of the Ten-VDAD.

Blocks >1 m in diameter are abundant in the Ten-VDAD, as exemplified in Fig. 2 and observed in other VDADs such as Augustine VDAD (Siebert et al., 1995) and the Parinacota VDAD (Clavero et al., 2002). Edifice blocks preserve their original stratigraphy and texture in locations 2 (Fig. 6) and 4 (Fig. 4). Furthermore, the abundance of undisaggregated jigsaw-fit clasts suggests high cohesion and low mixing (Ui et al., 2000). The preserved stratigraphy, jigsaw-fractured blocks, or even cataclased blocks with preserved outlines, suggest that large-scale turbulence and mixing can be excluded during the propagation of the Ten-VDA, as supported in other cases by Campbell et al. (1995), Reubi and Hernandez (2000), Voight et al. (2002) and Shea and van Wyk de Vries, (2008). Stratigraphic preservation indicates that the majority of the material experienced a frictional regime throughout the propagation (Manzella and Labiouse, 2013). In a collisional regime, where momentum transfer predominantly occurs through collisions (Iverson and Denlinger, 2001), the material would have experienced more disaggregation and mixing.

4.2. Local granular fluidal behaviour

Fluidal features such as clastic dikes (e.g. Fig. 5, 11d) and sporadic diffuse contacts (e.g. Fig. 8) between blocks and at the boundary between matrix-rich and block facies suggest a local granular fluid phase (van Wyk De Vries et al., 2001; Davies, 2015; van Wyk de Vries and Delcamp, 2015). Additionally, incomplete mixing offers evidence for agitated granular fluid behaviour in the matrix-rich facies (Fig. 9a-b) as suggested by van Wyk De Vries et al. (2001) in their study of the Socompa VDA. The preservation of blocks with intact stratigraphy overlying more fragmented material is not unusual in VDA/RA deposits (e.g. Erismann and Abele, 2001; Schilirò et al., 2019). Shearing features (Fig. 11) are also limited to block boundaries and lower outcrop sections.

Deeper in the Ten-VDAD, closer to the ravine floor, the convergence of normal faults, illustrated in Fig. 6, is the reason for the higher

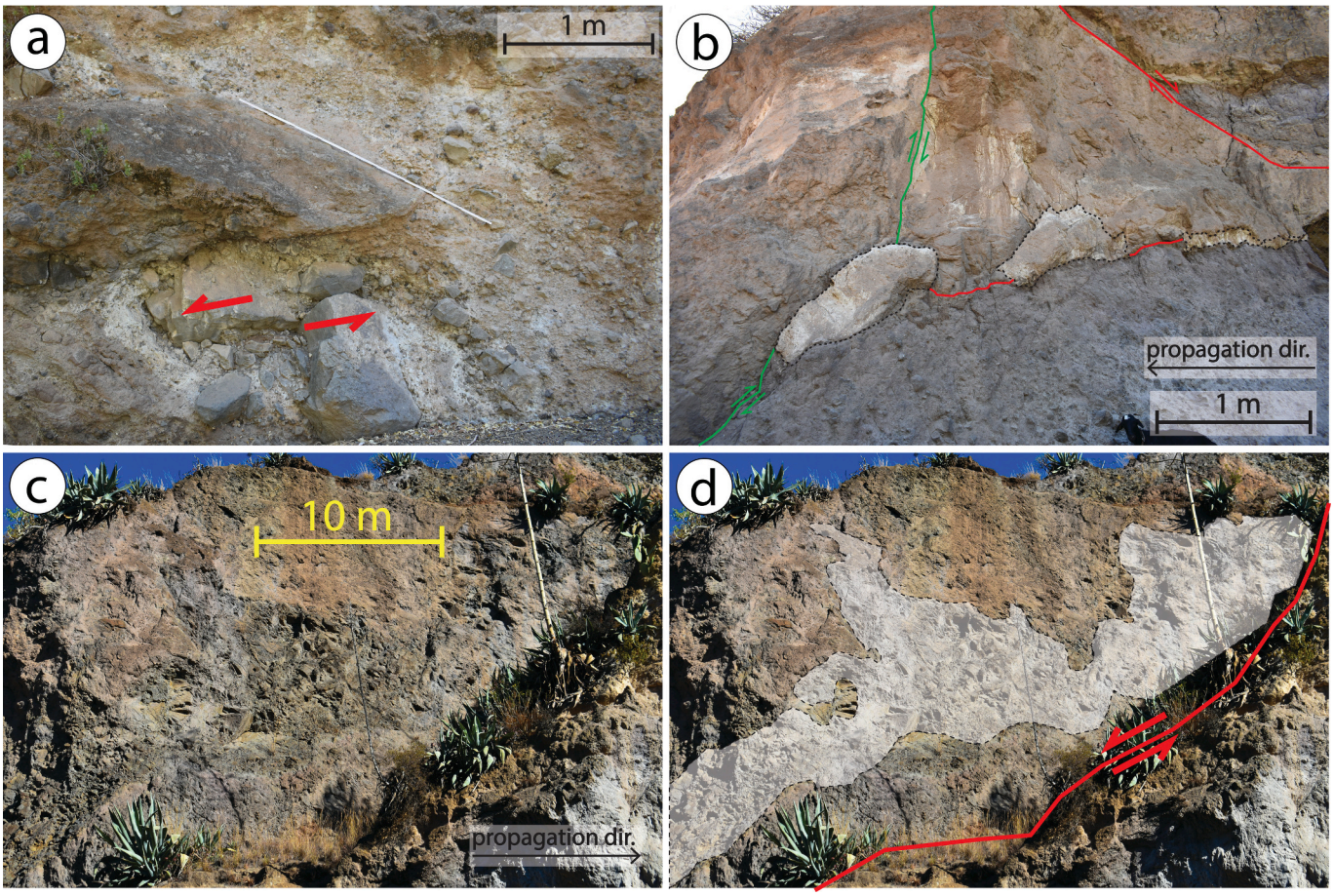

Fig. 11. Shear features of the Ten-VDAD. a Sheared clasts at the base of the exposure at location 5. b The outcrop at location 11 illustrates brittle deformation between components of the block facies. Red lines represent normal fault displacement, whereas green lines represent reverse fault displacement. Brittle shearband boudinage has been generated, illustrated by the boudins formed, orientated in the propagation direction. c Normal fault at block boundary at location 7. C and d represent the same location. d Flame injection and normal fault illustrate the shear accommodated at this zone. The displacement between the blocks generates the normal fault at the east of the outcrop illustrated in Fig. 2a and b. (For interpretation of the references to colour in this figure legend, the reader is referred to the web version of this article.)

disaggregation and poorer preservation of intact blocks. Convergence of the faults and the consequent higher shear stresses enable greater degrees of fracturing, thus leaving the mass more granular (as also predicted by the numerical model of Thompson et al. (2010) discussed in Section 4.3). As a result, component clasts can move independently, become agitated and interact in collisions after the initial post-collapse decompression and dilation (Fig. 12). This particle activity generates a granular temperature in these areas (Ogawa, 1978; Campbell, 1990; Iverson, 1997). The granular material interacts with the rough substrate to maintain a granular temperature (Cleary and Campbell, 1993; Iverson, 1997), which has even been suggested as capable of supporting the weight of the overriding material as a plug (e.g. Linares-Guerrero et al., 2007; Hu et al., 2021). Due to the granular temperature in the matrix as well as clasts in fractured block facies, the material behaves as an agitated granular fluidised mass (van Wyk De Vries et al., 2001; Thompson et al., 2009; Davies, 2015). The degree of agitation is low, if the flow remains laminar with low mixing, in accordance to the acoustic fluidisation theory as discussed by Collins and Melosh (2003). Although agitation was not great enough to generate turbulence, it did lead to relatively higher disaggregation of the material, and therefore, a reduction in preservation of stratigraphy and texture. This leads to the elimination of the jigsaw fabric by displacing component clasts (Campbell et al., 1995; Reubi and Hernandez, 2000; Clavero et al., 2002; Thompson et al., 2010), as illustrated in Fig. 3. The agitation vibrates and microdisplaces the material, resulting in the fine matrix intruding fractures within a block or clast, widening them and dispersing block/clast components (Fig. 3b). The material of the matrix-rich facies is initially injected in the block facies through the jigsaw fractures (Fig. 3b). Then clasts are separated and incorporated into the matrix (Fig. 3c-d) (Bernard et al., 2008; Roverato et al., 2015, 2018). As this occurs in blocks throughout the mass, this eventually leads to the mixing of lithologies observed in both the intrablock matrix (Fig. 7) as well as the matrix-rich facies (Fig. 3), and the gradual homogenisation of these domains, according to the process described by Roverato et al. (2015). Due to this process, the intrablock matrix is composed of the lithologies represented within a block. At the contacts, this diffusion process acts to add material from the outline of the block facies to the matrix-rich facies (Fig. 8a-b) (Bernard et al., 2008). The observation of a tendency for clasts of similar lithology to occur in groups in the matrix-rich facies of the Ten-VDAD, also made by Lomoschitz et al. (2008), is evidence of such fluid-like behaviour and gradual homogenisation at an incomplete stage (Fig. 9b).

The relatively higher degree of rounding (for example comparing the material in Fig. 7a, b with the material in Fig. 7c,d and 5a) of material in the matrix rich-facies and the intrablock matrix indicates abrasion during the viscous flow as suggested by Schneider and Fisher (1998). Fragmented particles are smoothed and rounded by frictional abrasion in the agitated mass (Schneider and Fisher, 1998; Perinotto et al., 2015; Paguican et al., 2021).

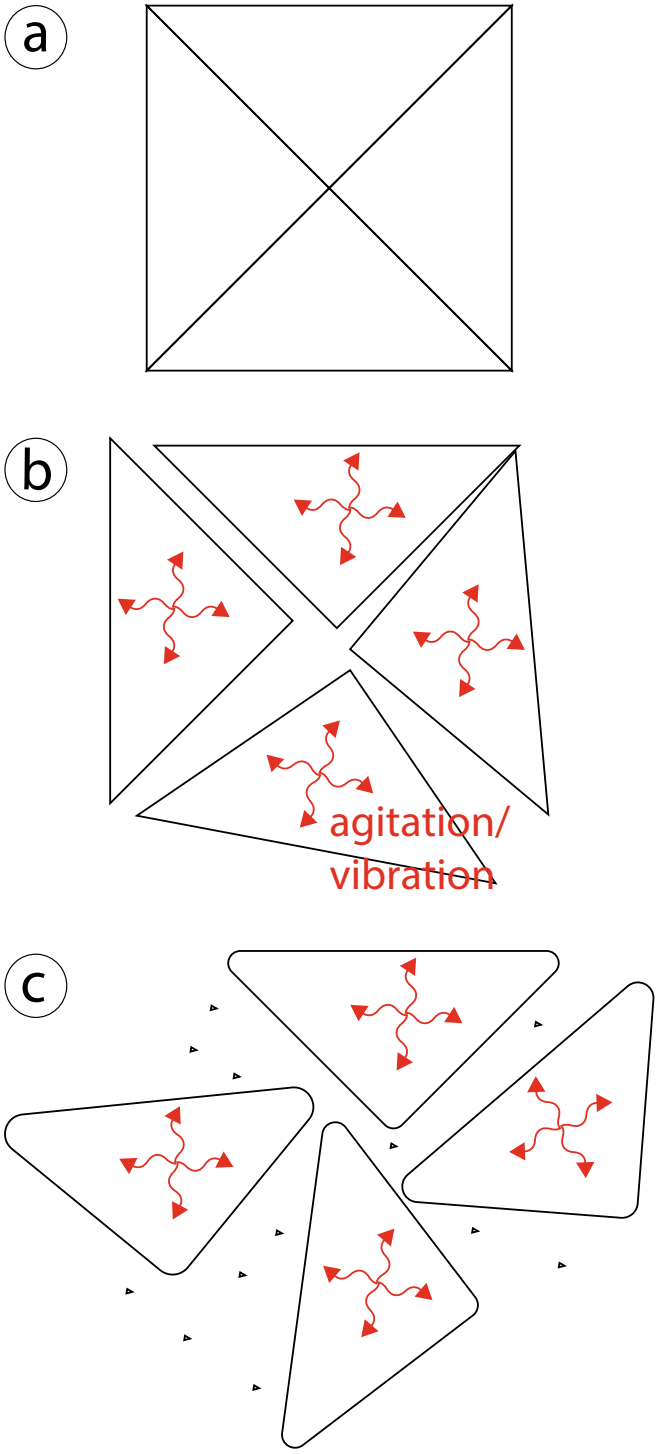

Fig. 12. Gradual disaggregation of jigsaw-fractured clasts/blocks due to agitation and granular temperature. a Jigsaw fractured material initially preserves the location of component parts and remains undisaggregated. b Vibration due to agitation displaces the particles relative to each other. c The original structure is progressively eliminated. Clasts become more rounded due to abrasion in their interactions, which also adds material to the matrix. The matrix fills the space between them to give the material a diamicton fabric. Diffuse contacts form where disaggregating clasts/blocks add material to the intrablock/interblock matrix.

4.3. Shear accommodation, propagation and emplacement model

VDAs result from flank collapses, propagating as slides immediately after the initial collapse and usually progressively evolve into flows (Voight et al., 1983; Siebert, 1984; Glicken, 1991; Scott et al., 2001). Mass fragmentation primarily occurs at the initial stages of edifice collapse due to decompression and dilation since the whole mass is in an extensional regime (Alidibirov and Dingwell, 1996; Longchamp et al., 2016) and the impact at the slope-break (Voight et al., 1983; Glicken, 1991, 1996; Bernard et al., 2008; Thompson et al., 2010). Subsequently, VDAs propagate further and progressive disaggregation continues (Roverato et al., 2015). Further fragmentation due to grain-to-grain contacts is thought to be minimal during propagation, and the generation of matrix is thought to be the result of disaggregation of already fractured material (e.g. Glicken, 1991; Palmer et al., 1991; Belousov et al., 1999; Bernard et al., 2008; Shea et al., 2008). Nonetheless, gradual abrasion of clasts in the more agitated regions can add small quantities of material to the matrix (Schneider and Fisher, 1998; Perinotto et al., 2015; Paguican et al., 2021). In the case of the Ten-VDA, the quantity of interblock matrix (Fig. 13) and degree of gradual homogenisation are low.

Distinct element numerical models by Thompson et al. (2010) have examined the propagation and emplacement of VDAs as granular avalanches where particles initially have a bond between them which can

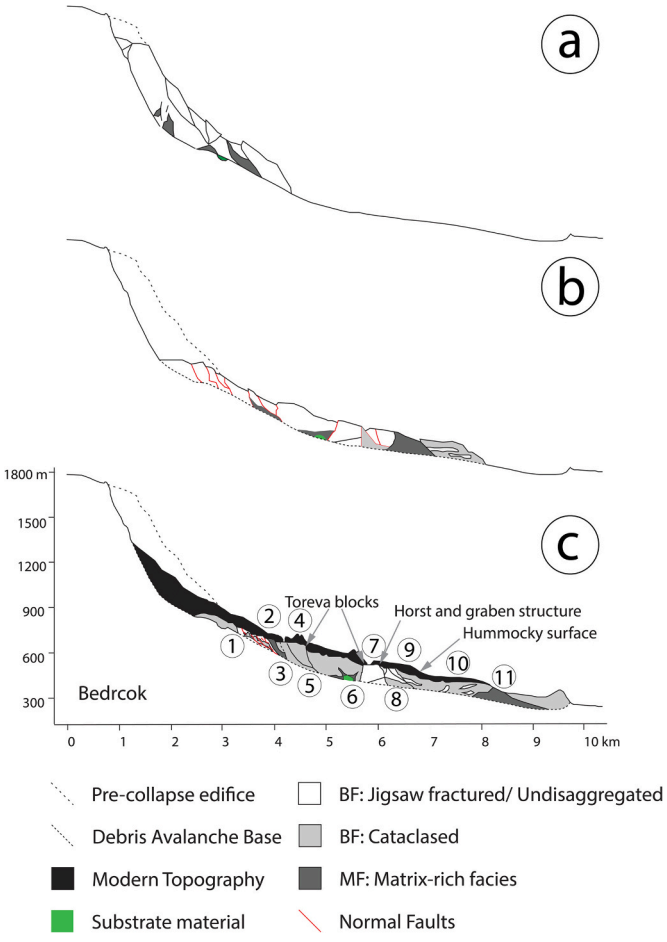

Fig. 13. Schematic representation of the propagation and emplacement of the Tenteniguada debris avalanche. a The initial stage of the collapse and coarse fracturing of the material. b Propagation stage where fractures are activated as normal faults to accommodate the spreading of the mass. c The final deposit with the features that have been observed in the field. Circled number represent the study locations as listed illustrated on the map in Fig. 1 and the table in the complementary material Appendix A.

be broken when their strength is overcome by local stresses during propagation. Subsequent evolution of the mass, as well as shear accommodation, are dependent on the distribution of the degree of disaggregation. Due to their potential to consider the strength of the material, such models are suitable for evaluating VDAs composed of relatively competent material, as is the case for the Ten-VDA. The model reproduces features observed in the Ten-VDAD, such as the normal fault generation and convergence, and allows the evaluation of propagation processes and dynamics.

The jigsaw-fractured pattern extensively exhibited by the Ten-VDAD (e.g. Fig. 2, 7a), has been suggested by Glicken (1996) to result from the expansion of a propagating mass at the initial collapse stage. Its preservation in the texture of the blocks in the interior of the proximal region of the Ten-VDAD suggests minimal agitation after the fracturing was generated by an impulsive force (Campbell et al., 1995; Schilirò et al., 2019). In agreement, the model of Thompson et al. (2010) suggests that the early stages of the collapse represent significant events for the fracturing and disaggregation of the mass. According to the model, during the initial collapse stress distribution is chaotic, however, the brittle failure initiating the fracturing of the mass, takes place even before the mass has evacuated the failure scarp. Analysis of the fractures of lava blocks in the Maronne Valley (Central Volcano, France) by Reubi and Hernandez (2000) also supports that fractures are primarily the result of shear stress at the initial stage of sliding. Fragmentation by rapid unloading is also supported by the pressure experimental findings of Alidibirov and Dingwell (1996). In the Ten-VDA this stage resulted in the coarse fracturing and large quantities of blocks observed in the deposit (e.g. Fig. 13a). Nonetheless, the existence of matrix-rich facies in proximal exposures (location 3) indicates that it was already generated from this early collapse stage. Therefore, the degree of mixing and disaggregation is not exclusively related to the distance from the source as also suggested by Bernard et al. (2008). Instead, it is also a function of the chaotic local stress distribution according to the instantaneous arrangement of the self-weight of the mass.

The abundance of normal faults at proximal areas and the interior of the deposit suggests that subsequent propagation-induced shear stresses were accommodated in fault zones (Fig. 13a). This regime allowed the spreading and back-tilting by rotational and sliding displacement of blocks, decreasing the avalanche thickness as exhibited, for example, at location 7 (Fig. 2). The blocks displaced in this way generate toreva features as illustrated in Fig. 13. In the Thompson et al. (2010) model, fractures generated during the initial collapse subsequently accommodate the spreading and resulting extension by activating as normal faults. The majority of the strain was accommodated in these shear zones and consequently, blocks were capable of preserving their internal stratigraphy (Thompson et al., 2010; Paguican, 2012). The model also predicts the observed large-scale toreva blocks in the medial area of the deposit (Fig. 13) under the definition of a massive portion of intact material that slid and back-tilted without being significantly brecciated (also observed by van Wyk De Vries et al., 2001; Clavero et al., 2002; Shea and van Wyk de Vries, 2008). This is observed in the proximal region of the Casana VDAD by Bustos et al. (2022). With progressive propagation, proximal and distal-facing normal faults generated the horst and graben complexes in the medial area of the Ten-VDAD, such as the one described in location 7 (Fig. 2).

Closer to the ravine floor, and in locations more distal than location 8, poorer preservation (Fig. 7c, d), more abundant intrablock matrix (Fig. 12) and scarcity of brittle features suggest higher stress accommodation. In the Thompson et al. (2010) model, faults conjoin at the base of the deposit generating a blockier upper portion; and a base with more matrix-rich facies and fewer large blocks, which are instead more cataclased. This aspect of the model is in agreement with the Ten-VDAD observation of more frequent preservation of blocks shallower in the deposit. Much of the deformation, fracturing and disaggregation of the mass has been concentrated and magnified deeper in the deposit, as exemplified at locations 2 and 4 (Figs. 4, 6).

The incorporation of a block from the substrate and inclusion as a clastic dyke (Fig. 5) occurred due to the shear of the substrate ploughing and detaching a section of the substrate (Dufresne et al., 2010a) and hosting it between two blocks. The built-up of pressure in the subsequent propagation forced part of the block in the fracture between the blocks generating the clastic dike. Gradual mixing enriched the surrounding matrix with substrate lithologies giving it a whiter colour (Fig. 5a).

Regarding the disaggregation of the distal areas of the Ten-VDAD, distal portions of granular flows experience acceleration and propagate for longer than the more proximal locations due to momentum transfer from material at the back to the front (Heim, 1932; Van Gassen and Cruden, 1989; Okura et al., 2000; Legros, 2002; Manzella and Labiouse, 2013; Bartali et al., 2015; Fan et al., 2016). Therefore, they are exposed to greater stress and for a longer time duration. During the emplacement phase, the proximal deposit decelerates faster, while the front of the VDA is still accelerating (Thompson et al., 2010). The process of momentum transfer imposes compressive stresses on the material at the front of the propagating mass (Longchamp et al., 2016; Hu et al., 2020). In the Ten-VDA, the higher disaggregation of the distal portion of the deposit could be the result of such amplified stress accommodation.

The fact that distinct normal fault planes are more abundant higher in the deposit, as illustrated in location 2 (Fig. 6), indicates the transition between the brittle behaviour to a relatively more liquefied/fluidised deeper in the Ten-VDA as suggested by Shea and van Wyk de Vries (2008). Nonetheless, the presence of a basal listric layer of major shear concentration could not be evaluated due to lack of exposure. Based on these observations, it can be assumed that two shear accommodation regimes have been active during the propagation of the Ten-VDA:

(1) In the more shallow domain of the deposit and in the proximal regions at the interior of the mass, the displacement was accommodated in normal faults between blocks, where shear was concentrated. Stress was not transmitted to the interior of blocks.
(2) Deeper in the deposit, where faults conjoined and stresses were higher, and at more distal locations, a regime of a relatively agitated granular flow is evident. In these areas, stress and agitation are distributed throughout the mass, causing the generation of more mixed and rounded material. Nonetheless, the flow regime remains laminar. It is most probable that particles adopted a behaviour between a rapid and quasistatic granular flow regime, rather than evolving into a pure rapid granular flow with a collisional regime (Campbell et al., 1995; Johnson et al., 2014).

Faults in the Thompson et al. (2010) model become progressively wider to facilitate the continuous spreading and extension, while the space is progressively filled by the increasing matrix-rich facies. The disaggregation allows the propagating mass to evolve into a fluidised granular flow. Deeper in the mass, in the model, the blocks are more likely to become disaggregated, and the material is stretched and thinned (Thompson et al., 2010). This is not observed in the Ten-VDAD, where matrix-rich facies is very scarce (Fig. 13c), suggesting that the deposit was emplaced before evolving to this stage of the rockslide-to-granular flow progression (Voight et al., 1983; Glicken, 1991). A dense network of blocks makes up the majority of the Ten-VDAD, with the matrix-rich facies limited to only a few areas between them (Fig. 13c). The Ten-VDA did not fully evolve from a slide to a flow (Voight et al., 1983; Glicken, 1991), and that is the reason it more closely resembles a non-volcanic blockslide deposit (Dufresne et al., 2010b).

For a VDA to evolve into a flow stresses need to overcome the strength of the propagating material in order to disaggregate the mass (Thompson et al., 2010). Once the majority of the mass can behave as a granular flow it is believed to assume the typical VDA flow behaviour (Voight et al., 1983; Glicken, 1996; Schneider and Fisher, 1998; Thompson et al., 2009). This has not been achieved by the Ten-VDA

primarily because of the competent nature of the lava lithologies that compose the majority of the material. Other potential factors for the primarily brittle behaviour are: the low volume relative to other VDAs (Legros, 2002), the low slope of the path, and potential substrate interactions. Lomoschitz et al. (2008) suggest that the emplacement of the Ten-VDA might have also been aided by the topographic high where its toe has been deposited (Fig. 13).

Nevertheless, considering that the Ten-VDA has achieved an H/L ratio of ~0.16 implies that it attained much greater horizontal runout distance compared to its initial fall height (Fig. 14a). Given the runout and the low degree of disaggregation observed in the deposit two candidate processes can be proposed for the Ten-VDA propagation:

(1) Normal faults and extensional features illustrate extensive spreading and lowering. Therefore, one explanation for the long runout of the Ten-VDA is the spreading of the mass. This implies that the material spread, lowering its centre of mass and pushing the front of the material further. This behaviour in granular material provides increased runout without increased mobility of the centre of mass (Fig. 14) (Legros, 2002; Manzella and Labiouse, 2013). Therefore, no mechanism is required to explain reduced friction that would result in greater displacement of its centre of mass. In such a case, the runout is the result of normal fault-accommodated spreading. Spreading has been proposed as a theory for the excessive runout of VDAs/RAs by Davies (1982) and Davies and McSaveney (1999). In fact, this process highlights the mechanical irrelevance of the H/L as a measure of mobility, since spreading generates a higher runout which is not necessarily reflected in the mobility of the centre of mass, and therefore energy dissipation (Davies, 1982; Legros, 2002; Dufresne et al., 2021a).

(2) The lack of major shear accommodation in the body of the Ten-VDA could imply shear concentration in a basal listric layer. Shear concentration in a low frictional basal layer can result in reduced frictional losses and increased mobility (Fig. 14b). In avalanches composed of weaker material, where disaggregation is more intense, a basal shear layer is more likely to develop (Thompson et al., 2009). The convergence of faults and more fractured material at the base of the Ten-VDA might have allowed to evolve into a valley-confined plug flow if enough fractured/disaggregated material was generated at the base to allow local fluid granular behaviour (Paguican et al., 2021). In this case, the material at the interior of the flow would have travelled as a coherent plug over a basal and marginal low friction shear zone acting as a Bingham fluid (Voight et al., 1983; Takarada et al., 1999; Paguican et al., 2021). Takarada et al. (1999) suggest that this can be encouraged by greater proportions of weaker or hydrothermally altered lithologies since a significant amount of matrix is required to support the overlying material and initiate the plug flow phase (Paguican et al., 2021). However, large amounts of matrix are not observed in the Ten-VDAD (Fig. 13). Consequently, deformation and shear have to be distributed through the avalanche body. Although the confinement by the paleoravine could encourage this process, the lack of weaker material that could be easily disaggregated is likely to have impeded the Ten-VDA from evolving into a plug flow on a low friction basal zone.

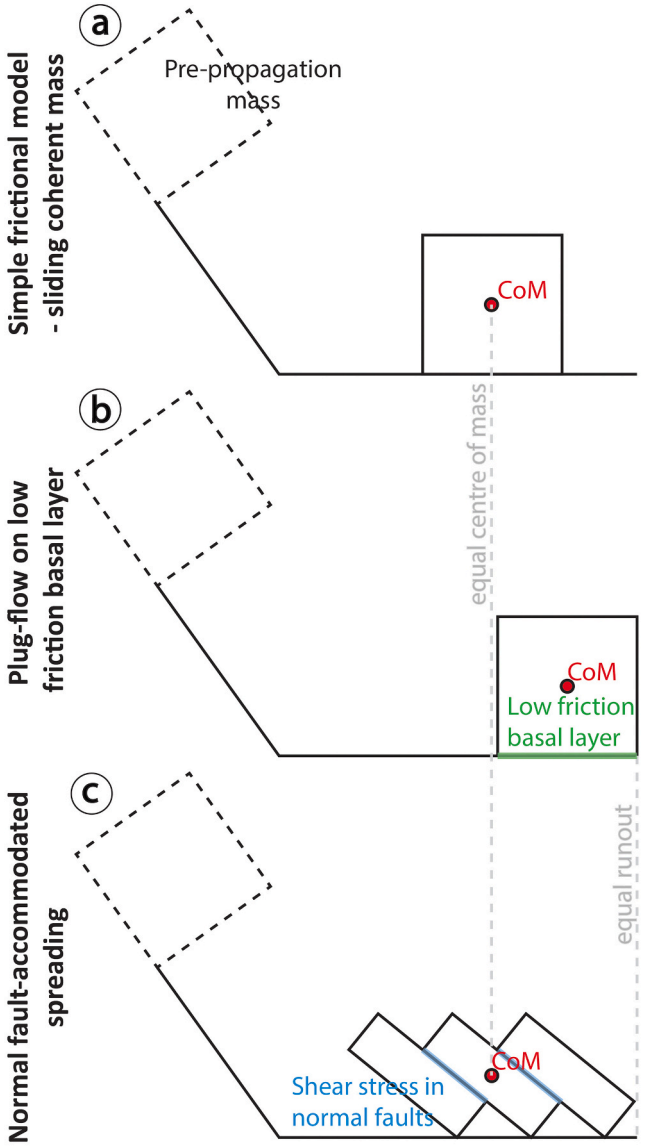

Fig. 14. a Displacement of a mass after propagation, assuming a simple frictional model of a coherent sliding mass. b Plug-flow on a low friction basal layer: due to a reduction of friction the mass propagates further resulting in a longer runout and displacement of the centre of mass (CoM). c Normal fault-accommodated spreading: Spreading and extension of the mass results in a longer runout compared to a, while the displacement of the CoM remains unchanged. Back-tilting of blocks and activation of normal faults observed in the field is also consistent with this simple model.

The lack of exposure of the base of the Ten-VDA does not permit a conclusive evaluation of the two hypotheses. However, the low degree of disaggregation and quantity of matrix in the exposed sections suggest that extensive basal shear accommodation is unlikely. It is, therefore, proposed that the mobility of the Ten-VDA was enabled by the normal fault-accommodated spreading of the mass by the extensional displacement of normal faults between blocks. This mechanism is also in agreement with the observations of undisaggregated blocks and brittle features since most of the shear of the displacement was accommodated in normal faults for the spreading of the mass, resulting in the lack of strain in the interior of blocks.

5. Conclusion

The facies distribution and structural analysis have led to the following model for the propagation and emplacement of the Ten-VDA:

1. The collapsed portion of the source edifice did not suffer a high degree of alteration and weakening that would precondition the mass for fracturing. Therefore, in the initial collapse and slide phase, evolution of fractures, and coarse disaggregation of the mass were initiated but a major component of undisaggregated blocks was preserved (Fig. 13a).

2. In the subsequent propagation, extension and spreading were accommodated in normal faulting activated in pre-existing fractures (Fig. 13b). This led to shearing in the fault zones and back-tilting of blocks (Figs. 6, 11).
3. Extension and lowering of the mass progressed, with disaggregation of blocks and matrix injected in fractures between blocks. In the matrix-rich facies, there was no turbulence or shearing and mixing was limited to gradual homogenisation generated by the agitation due to granular temperature (Fig. 12). The VDA remained cohesive, as a dense network of blocks. Blocks were cataclased to various degrees but preserved their outline and distinct lithological composition. The cataclasis of the blocks generated a fine intrablock matrix, however, interblock mixing was limited to a small quantity of diffuse boundaries. Horst and graben structures developed as the extension proceeded (Fig. 2, 13b).
4. Deeper in the deposit, the faults conjoin. There was a higher degree of shearing and agitation. Disaggregation and intrablock matrix generation were higher, eliminating jigsaw fracturing and imposing a diamicton fabric to the block facies. There was also a small amount of substrate incorporation.
5. The more distal part of the Ten-VDA exhibits higher disaggregation and gradual mixing due to agitation. This is the result of the higher stresses accommodated at the front for a longer duration due to the momentum transfer from the back and longer runout.
6. The poor disaggregation of the mass, large component of block facies and poor mixing between blocks suggest that the Ten-VDA did not fully evolve to a flow. A brittle type behaviour was dominant. The resultant deposit is comprised of a dense network of blocks.

The lack of exposure of the base of the landslide does not allow the assessment of the degree of shear accommodation at the base and the nature of the interaction with the substrate. Therefore, the excess mobility of the Ten-VDA could be attributed to two candidate processes: 1. The mobility could be the result of normal fault-accommodated spreading and extension of the mass. In this case, the increased runout would be the result of the spreading of the material, while the centre of mass would not necessarily have achieved a high mobility (Fig. 14c). 2. Alternatively, a low-friction basal layer might have accommodated the shear of the displacement, supporting the material above, which would have travelled as a plug-flow on a low-friction basal layer (Fig. 14b) (sensu Takarada et al., 1999). The first process appears more likely due to the brittle behaviour of the material and lack of extensive quantities of matrix-rich facies. Although unlikely, the second process cannot be definitively rejected due to the lack of exposure of the deposit base.

The present study demonstrates the importance of detailed field observations to assess mechanisms affecting the mobility of VDA and puts in evidence how different process are possible and should be taken into consideration when assessing the hazard related to these phenomena.

Funding

The authors are grateful to the Geological Society of London for funding the fieldwork for this study through a Research Grant.

CRediT authorship contribution statement

Symeon Makris: Conceptualization, Investigation, Methodology, Visualization, Funding acquisition, Writing – original draft. **Matteo Roverato:** Conceptualization, Investigation, Methodology, Writing – review & editing. **Alejandro Lomoschitz:** Investigation, Writing – review & editing. **Paul Cole:** Conceptualization, Investigation, Writing – review & editing. **Irene Manzella:** Conceptualization, Investigation, Supervision, Funding acquisition, Writing – review & editing.

Declaration of Competing Interest

The authors declare that they have no known competing financial interests or personal relationships that could have appeared to influence the work reported in this paper.

Data availability

Data will be made available on request.

Acknowledgements

The authors would like to thank Dr. José Luis Macías and two anonymous reviewers for their in-depth review and comments that considerably improved this paper.

Appendix A. Supplementary data

Supplementary data to this article can be found online at https://doi.org/10.1016/j.jvolgeores.2023.107773.

References

Alidibirov, M., Dingwell, D.B., 1996. Magma fragmentation by rapid decompression. Nature 380, 146–148.
Balcells, R., Barrera, J., Gómez, J., 1990. Mapa Geológico de España a escala 1: 25,000 Gran Canaria, Maps 1109 II (Telde) and 1109 III (San Bartolomé de Tirajana).
Banton, J., Villard, P., Jongmans, D., Scavia, C., 2009. Two-dimensional discrete element models of debris avalanches: parameterization and the reproducibility of experimental results. J. Geophys. Res. Earth Surf. 114, 1–15. https://doi.org/10.1029/2008JF001161.
Bartali, R., Sarocchi, D., Nahmad-Molinari, Y., 2015. Stick-slip motion and high speed ejecta in granular avalanches detected through a multi-sensors flume. Eng. Geol. 195, 248–257. https://doi.org/10.1016/j.enggeo.2015.06.019.
Belousov, A., Belousova, M., Voight, B., 1999. Multiple edifice failures, debris avalanches and associated eruptions in the Holocene history of Shiveluch volcano, Kamchatka, Russia. Bull. Volcanol. 61, 324–342. https://doi.org/10.1007/s004450050300.
Bernard, B., van Wyk de Vries, B., Barba, D., Leyrit, H., Robin, C., Alcaraz, S., et al., 2008. The Chimborazo sector collapse and debris avalanche: deposit characteristics as evidence of emplacement mechanisms. J. Volcanol. Geotherm. Res. 176, 36–43. https://doi.org/10.1016/j.jvolgeores.2008.03.012.
Bernard, B., Takarada, S., Andrade, S.D., Dufresne, A., 2021. Terminology and strategy to describe large volcanic landslides and debris avalanches. In: Roverato, M., Dufresne, A., Procter, J. (Eds.), Volcanic Debris Avalanches: From Collapse to Hazard. Springer book series advances in volcanology, pp. 51–73.
Bustos, E., Capra, L.M.A., Norini, G., 2022. Volcanic debris avalanche transport and emplacement at Chimpa volcano (Central Puna, Argentina): insights from morphology, grain-size and clast surficial textures. J. Volcanol. Geotherm. Res. https://doi.org/10.1016/j.jvolgeores.2022.107671.
Campbell, C.S., 1989. Self-lubrication for long runout landslides. J. Geol. 97, 653–665.
Campbell, C.S., 1990. Rapid granular flows. Annu. Rev. Fluid Mech. 22, 57–90.
Campbell, C.S., Cleary, P.W., Hopkins, M., 1995. Large-scale landslide simulations: global deformation, velocities and basal friction. J. Geophys. Res. 100, 8267–8283. https://doi.org/10.1029/94JB00937.
Capra, L., Macías, J.L., Scott, K.M., Abrams, M., Garduño-Monroy, V.H., 2002. Debris avalanches and debris flows transformed from collapses in the Trans-Mexican Volcanic Belt, Mexico - Behavior, and implications for hazard assessment. J. Volcanol. Geotherm. Res. 113, 81–110. https://doi.org/10.1016/S0377-0273(01)00252-9.
Clavero, J., Sparks, R., Huppert, H., Dade, W., 2002. Geological constraints on the emplacement mechanism of the Parinacota debris avalanche, Northern Chile. Bull. Volcanol. 64, 40–54. https://doi.org/10.1007/s00445-001-0183-0.
Cleary, P.W., Campbell, C.S., 1993. Self-lubrication for long runout landslides: examination by computer simulation. J. Geophys. Res. Solid Earth 98, 21911–21924.
Collins, G.S., Melosh, H.J., 2003. Acoustic fluidization and the extraordinary mobility of sturzstroms. J. Geophys. Res. Solid Earth 108, 1–14. https://doi.org/10.1029/2003jb002465.
Cruden, D.M., Varnes, D.J., 1996. Landslide types and processes. In: Turner, A.K., Schuster, R.L. (Eds.), Landslides-Investigation and Mitigation. National Academy Press, Washington DC, pp. 36–75. Transportation Research Board Special Report 247,.
Davies, T., 1982. Spreading of rock avalanche debris by mechanical fluidization. Rock Mech. 24, 9–24.
Davies, T., 2015. Hazards and Disasters Series Landslide Hazards, Risks, and Disasters. https://doi.org/10.1016/B978-0-12-394846-5.01001-8.
Davies, T., McSaveney, M.J., 1999. Runout of dry granular avalanches. Can. Geotech. J. https://doi.org/10.1139/t98-108.
Davies, T., McSaveney, M., 2012. Mobility of long-runout rock avalanches. In: Stead, J.J. Clague D. (Ed.), Landslides–types, Mech. Model, pp. 50–58.

Delcamp, A., Kervyn, M., Benbakkar, M., Kwelwa, S., Peter, D., 2017. Large volcanic landslide and debris avalanche deposit at Meru, Tanzania. Landslides 14, 833–847. https://doi.org/10.1007/s10346-016-0757-8.

Dufresne, A., Dunning, S., 2017. Process dependence of grain size distributions in rock avalanche deposits. Landslides 14, 1555–1563. https://doi.org/10.1007/s10346-017-0806-y.

Dufresne, A., Davies, T., McSaveney, M.J., 2010a. Influence of runout-path material on emplacement of the Round Top rock avalanche, New Zealand. Earth Surf. Process. Landf. 35, 190–201. https://doi.org/10.1002/esp.1900.

Dufresne, A., Salinas, S., Siebe, C., 2010b. Substrate deformation associated with the Jocotitlán edifice collapse and debris avalanche deposit, Central México. J. Volcanol. Geotherm. Res. 197, 133–148. https://doi.org/10.1016/j.jvolgeores.2010.02.019.

Dufresne, A., Prager, C., Bösmeier, A., 2016. Insights into rock avalanche emplacement processes from detailed morpho-lithological studies of the Tschirgant deposit (Tyrol, Austria). Earth Surf. Process. Landf. 41, 587–602. https://doi.org/10.1002/esp.3847.

Dufresne, A., Siebert, L., Bernard, B., 2021a. Distribution and geometric parameters of volcanic debris avalanche deposits. In: Volcanic Debris Avalanches. Springer, pp. 75–90.

Dufresne, A., Zernack, A., Bernard, K., Thouret, J.-C., Roverato, M., 2021b. Sedimentology of volcanic debris avalanche deposits. In: Roverato, M., Dufresne, A., Procter, J. (Eds.), Volcanic Debris Avalanches: From Collapse to Hazard. Springer book series advances in volcanology, Cham, pp. 175–210. https://doi.org/10.1007/978-3-030-57411-6_8.

Erismann, T.H., 1979. Mechanisms of large landslides. In: Rock Mech. Felsmechanik Mécanique des Roches. https://doi.org/10.1007/BF01241087.

Erismann, T.H., Abele, G., 2001. Dynamics of Rockslides and Rockfalls. Springer Science & Business Media. https://doi.org/10.1017/CBO9781107415324.004.

Fan, X., Tian, S., Zhang, Y., 2016. Mass-front velocity of dry granular flows influenced by the angle of the slope to the runout plane and particle size gradation. J. Mt. Sci. 13, 234–245. Available at: https://doi.org/10.1007/s11629-014-3396-3.

Funck, T., Schmincke, H.-U., 1998. Growth and destruction of Gran Canaria deduced from seismic reflection and bathymetric data. J. Geophys. Res. Solid Earth 103, 15393–15407.

Glicken, H., 1991. Sedimentary architecture of large volcanic-debris avalanches. In: Sedimentation in Volcanic Settings, pp. 99–106. https://doi.org/10.2110/pec.91.45.0099.

Glicken, H., 1996. Rockslide-Debris Avalanche of May 18, 1980, Mount St. Helens Volcano, Washington. USGS Open File Report 96-677. Bull. Surv.

Goscombe, B.D., Passchier, C.W., Hand, M., 2004. Boudinage classification: end-member boudin types and modified boudin structures. J. Struct. Geol. 26, 739–763. https://doi.org/10.1016/j.jsg.2003.08.015.

Heim, A., 1932. Bergsturz und menschenleben. Fretz & Wasmuth, p. 77.

Hu, Y. Xiang, Li, H. Bo, Qi, S. Chao, Fan, G., Zhou, J. Wen, 2020. Granular Effects on Depositional Processes of Debris Avalanches. KSCE J. Civ. Eng. 24, 1116–1127. https://doi.org/10.1007/s12205-020-1555-3.

Hu, Y. Xiang, Li, H. Bo, da Lu, G., Fan, G., Zhou, J. Wen, 2021. Influence of size gradation on particle separation and the motion behaviors of debris avalanches. Landslides. https://doi.org/10.1007/s10346-020-01596-z.

Hürlimann, M., Ledesma, A., 2003. Giant mass movements in Volcanic Islands: The case of Tenerife. In: Occurence and Mechanisms of Flow-Like Landslides in Natural Slopes and Earthfills (Sorrento), pp. 105–115.

Iverson, R., 1997. The physics of debris flows. Rev. Geophys. 35, 245–296. https://doi.org/10.1029/97RG00426.

Iverson, R., Denlinger, R.P., 2001. Flow of variably fluidized granular masses across three-dimensional terrain: 1. Coulomb mixture theory. J. Geophys. Res. Solid Earth. https://doi.org/10.1029/2000JB900329.

Johnson, B.C., Campbell, C.S., Melosh, J.H., 2014. The reduction of friction in long runout landslides as an emergent phenomenon. J. Geophys. Res. Earth Surf. 300–316 https://doi.org/10.1002/2013JF002871.

Legros, F., 2002. The mobility of long-runout landslides. Eng. Geol. 63, 301–331. https://doi.org/10.1016/S0013-7952(01)00090-4.

Linares-Guerrero, E., Goujon, C., Zenit, R., 2007. Increased mobility of bidisperse granular avalanches. J. Fluid Mech. 593, 475–504. https://doi.org/10.1017/S0022112007008932.

Lomoschitz, A., Hervás, J., Yepes, J., Meco, J., 2008. Characterisation of a pleistocene debris-avalanche deposit in the Tenteniguada Basin, Gran Canaria Island, Spain. Landslides 5, 227–234. https://doi.org/10.1007/s10346-008-0115-6.

Longchamp, C., Abellan, A., Jaboyedoff, M., Manzella, I., 2016. 3-D models and structural analysis of rock avalanches: the study of the deformation process to better understand the propagation mechanism. Earth Surf. Dyn. 4, 743–755. https://doi.org/10.5194/esurf-4-743-2016.

Makris, S., Manzella, I., Cole, P., Roverato, M., 2020. Grain size distribution and sedimentology in volcanic mass-wasting flows: implications for propagation and mobility. Int. J. Earth Sci. https://doi.org/10.1007/s00531-020-01907-8.

Manzella, I., Labiouse, V., 2013. Empirical and analytical analyses of laboratory granular flows to investigate rock avalanche propagation. Landslides 10, 23–36. https://doi.org/10.1007/s10346-011-0313-5.

Meco, J., Guillou, H., Carracedo, J.-C., Lomoschitz, A., Ramos, A.-J.G., Rodríguez-Yánez, J.-J., 2002. The maximum warmings of the Pleistocene world climate recorded in the Canary Islands. Palaeogeogr. Palaeoclimatol. Palaeoecol. 185, 197–210.

Meco, J., Petit-Maire, N., Guillou, H., Carracedo, J.C., Lomoschitz, A., Ramos, A.J.G., et al., 2003. Climatic changes over the last 5,000,000 years as recorded in the Canary Islands. 地质幕 英文版 26, 133–134.

Mehl, K.W., Schmincke, H.U., 1999. Structure and emplacement of the Pliocene Roque Nublo debris avalanche deposit, Gran Canaria, Spain. J. Volcanol. Geotherm. Res. 94, 105–134. https://doi.org/10.1016/S0377-0273(99)00100-6.

Ogawa, S., 1978. Multitemperature theory of granular materials. In: Proc. of the US-Japan Seminar on Continuum Mechanical and Statistical Approaches in the Mechanics of Granular Materials, 1978, pp. 208–217.

Okura, Y., Kitahara, H., Sammori, T., Kawanami, A., 2000. Effects of rockfall volume on runout distance. Eng. Geol. 58, 109–124. https://doi.org/10.1016/S0013-7952(00)00049-1.

Paguican, E.M., 2012. The structure, morphology, and surface texture of debris avalanche deposits: Eld and remote sensing mapping and analogue modelling. Available at. file:///C:/Users/Michael/AppData/Local/Temp/The_Structure_Morphology_and_Surface_Texture_of_De.pdf.

Paguican, E.M., Roverato, M., Yoshida, H., 2021. Volcanic debris avalanche transport and emplacement mechanisms. In: Roverato, M., Dufresne, A., Procter, J. (Eds.), Volcanic Debris Avalanches: From Collapse to Hazard. Springer book series advances in volcanology, pp. 143–173. https://doi.org/10.1007/978-3-030-57411-6_7.

Palmer, B., Alloway, B., Vincent, N., 1991. Volcanic-debris-avalanche deposits in New Zealand—Lithofacies organization in unconfined, wet-avalanche flows. In: Sediment. Volcan. Settings, 89–98. https://doi.org/10.2110/pec.91.45.0089.

Perez-Torrado, F.J., Carracedo, J.C., Mangas, J., 1995. Geochronology and stratigraphy of the Roque Nublo Cycle, Gran Canaria, Canary Islands. J. Geol. Soc. 152, 807–818. https://doi.org/10.1144/gsjgs.152.5.0807.

Perinotto, H., Schneider, J.L., Bachèlery, P., Le Bourdonnec, F.X., Famin, V., Michon, L., 2015. The extreme mobility of debris avalanches: a new model of transport mechanism. J. Geophys. Res. Solid Earth. https://doi.org/10.1002/2015JB011994.

Pollet, N., Schneider, J.L.M., 2004. Dynamic disintegration processes accompanying transport of the Holocene Flims sturzstrom (Swiss Alps). Earth Planet. Sci. Lett. 221, 433–448. https://doi.org/10.1016/S0012-821X(04)00071-8.

Pudasaini, S.P., Hutter, K., 2007. Avalanche Dynamics: Dynamics of Rapid Flows of Dense Granular Avalanches. Springer Science & Business Media.

Quintana, A., Lomoschitz, A., 2005. Characterisation of a debris avalanche deposit based on its geomorphic and internal features. In: Tenteniguada Basin, Gran Canaria (Spain). Abstr. 6th Int. Conf. Geomorphol. Zaragoza, Spain, p. 313.

Reubi, O., Hernandez, J., 2000. Volcanic debris avalanche deposits of the upper Maronne valley (Cantal Volcano, France): evidence for contrasted formation and transport mechanisms. J. Volcanol. Geotherm. Res. 102, 271–286. https://doi.org/10.1016/S0377-0273(00)00191-8.

Roberti, G., Friele, P., van Wyk de Vries, B., Ward, B., Clague, J.J., Perotti, L., et al., 2017. Rheological evolution of the mount meager 2010 debris avalanche, southwestern British columbia. Geosphere 13, 1–22. https://doi.org/10.1130/GES01389.1.

Roverato, M., Capra, L., 2013. Características microtexturales como indicadores del transporte y emplazamiento de dos depósitos de avalancha de escombros del Volcán de Colima (México).pdf, pp. 512–525.

Roverato, M., Dufresne, A., 2021. Volcanic debris avalanches: Introduction and book structure. In: Roverato, M., Dufresne, A., Procter, J. (Eds.), Volcanic Debris Avalanches: From Collapse to Hazard. Springerbook series advances in volcanology, pp. 1–10.

Roverato, M., Capra, L., Sulpizio, R., Norini, G., 2011. Stratigraphic reconstruction of two debris avalanche deposits at Colima Volcano (Mexico): insights into pre-failure conditions and climate influence. J. Volcanol. Geotherm. Res. 207, 33–46. https://doi.org/10.1016/j.jvolgeores.2011.07.003.

Roverato, M., Cronin, S., Procter, J., Capra, L., 2015. Textural features as indicators of debris avalanche transport and emplacement, Taranaki volcano. Bull. Geol. Soc. Am. 127, 3–18. https://doi.org/10.1130/B30946.1.

Roverato, M., Larrea, P., Casado, I., Mulas, M., Béjar, G., Bowman, L., 2018. Characterization of the Cubilche debris avalanche deposit, a controversial case from the northern Andes, Ecuador. J. Volcanol. Geotherm. Res. https://doi.org/10.1016/j.jvolgeores.2018.07.006.

Roverato, M., Di Traglia, F., Procter, J., Paguican, E., Dufresne, A., 2021. Factors contributing to volcano lateral collapse. In: Roverato, M., Dufresne, A., Procter, J. (Eds.), Volcanic Debris Avalanches: From Collapse to Hazard. Springer book series advances in volcanology, pp. 91–119.

Schilirò, L., Esposito, C., De Blasio, F.V., Scarascia Mugnozza, G., 2019. Sediment texture in rock avalanche deposits: insights from field and experimental observations. Landslides 16, 1629–1643. https://doi.org/10.1007/s10346-019-01210-x.

Schneider, J.L., Fisher, R.V., 1998. Transport and emplacement mechanisms of large volcanic debris avalanches: evidence from the northwest sector of Cantal Volcano (France). J. Volcanol. Geotherm. Res. 83, 141–165. https://doi.org/10.1016/S0377-0273(98)00016-X.

Scott, K., Macias, J.L., Naranjo, J.A., Rodriguez, S., McGeehin, J.P., 2001. Catastrophic debris flows transformed from landslides in volcanic terrains: Mobility, hazard assessment, and mitigation strategies. Available at. http://www.scopus.com/scopus/inward/record.url?eid=2-s2.0-0003273447&partner=40&rel=R4.5.0.

Shea, T., van Wyk de Vries, B., 2008. Structural analysis and analogue modeling of the kinematics and dynamics of rockslide avalanches. Geosphere 4, 657–686. https://doi.org/10.1130/GES00131.1.

Shea, T., van Wyk de Vries, B., Pilato, M., 2008. Emplacement mechanisms of contrasting debris avalanches at Volcán Mombacho (Nicaragua), provided by structural and facies analysis. Bull. Volcanol. 70, 899–921. https://doi.org/10.1007/s00445-007-0177-7.

Shreve, R.L., 1968. The Blackhawk Landslide. Geol. Soc. Am. Spec. Pap, p. 108.

Siebe, C., Komorowski, J.-C., Sheridan, M.F., 1992. Morphology and emplacement of an unusual debris-avalanche deposit at Jocotitlán volcano, Central Mexico. Bull. Volcanol. 54, 573–589. https://doi.org/10.1007/BF00569941.

Siebert, L., 1984. Large volcanic debris avalanches: Characteristics of source areas, deposits, and associated eruptions. J. Volcanol. Geotherm. Res. 22, 163–197. https://doi.org/10.1016/0377-0273(84)90002-7.

Siebert, L., Roverato, M., 2021. A historical perspective on lateral collapse and volcanic debris avalanches. In: Roverato, M., Dufresne, A., Procter, J. (Eds.), Volcanic Debris Avalanches: From Collapse to Hazard. Springer book series advances in volcanology, pp. 11–50.

Siebert, L., Begét, J.E., Glicken, H., 1995. The 1883 and late-prehistoric eruptions of Augustine volcano, Alaska. J. Volcanol. Geotherm. Res. 66, 367–395. https://doi.org/10.1016/0377-0273(94)00069-S.

Siebert, L., Alvarado, G.E., Vallance, J.W., De Vries, Van Wyk, B., 2006. Large-volume volcanic edifi ce failures in Central America and associated hazards. Spec. Pap. Geol. Soc. Am. 412, 1–26. https://doi.org/10.1130/2006.2412(01).

Smyth, M., 1991. Movement and emplacement mechanisms of the Rio Pita Volcanic Debris Avalanche and its role in the evolution of Cotopaxi Volcano. In: ProQuest LLC 2014.

Takarada, S., Ui, T., Yamamoto, Y., 1999. Depositional features and transportation mechanism of valley-filling Iwasegawa and Kaida debris avalanches, Japan. Bull. Volcanol. 60, 508–522.

Thompson, N., Bennett, M.R., Petford, N., 2009. Analyses on granular mass movement mechanics and deformation with distinct element numerical modeling: implications for large-scale rock and debris avalanches. Acta Geotech. 4, 233–247. https://doi.org/10.1007/s11440-009-0093-4.

Thompson, N., Bennett, M.R., Petford, N., 2010. Development of characteristic volcanic debris avalanche deposit structures: new insight from distinct element simulations. J. Volcanol. Geotherm. Res. 192, 191–200. https://doi.org/10.1016/j.jvolgeores.2010.02.021.

Ui, T., 1983. Volcanic dry avalanche deposits - Identification and comparison with nonvolcanic debris stream deposits. J. Volcanol. Geotherm. Res. 18, 135–150. https://doi.org/10.1016/0377-0273(83)90006-9.

Ui, T., 1989. Discrimination Between Debris Avalanches and Other Volcaniclastic Deposits, pp. 201–209. https://doi.org/10.1007/978-3-642-73759-6_13.

Ui, T., Takarada, S., Yashimoto, M., 2000. Debris avalanches. In: Sigurdsson, H. (Ed.), Encyclopedia of Volcanoes. Academic Press, San Diego, pp. 617–626.

Van Gassen, W., Cruden, D.M., 1989. Momentum transfer and friction in the debris of rock avalanches. https://doi.org/10.1139/t89-075.

van Wyk de Vries, B., Delcamp, A., 2015. Volcanic Debris Avalanches. Elsevier Inc. https://doi.org/10.1016/B978-0-12-396452-6.00005-7.

van Wyk De Vries, B., Self, S., Francis, P.W., Keszthelyi, L., 2001. A gravitational spreading origin for the Socompa debris avalanche. J. Volcanol. Geotherm. Res. 105, 225–247. https://doi.org/10.1016/S0377-0273(00)00252-3.

Vezzoli, L., Apuani, T., Corazzato, C., Uttini, A., 2017. Geological and geotechnical characterization of the debris avalanche and pyroclastic deposits of Cotopaxi Volcano (Ecuador). A contribute to instability-related hazard studies. J. Volcanol. Geotherm. Res. 332, 51–70. https://doi.org/10.1016/j.jvolgeores.2017.01.004.

Voight, B., 2000. Structural stability of andesite volcanoes and lava domes. Philos. Trans. R. Soc. London. Ser. A Math. Phys. Eng. Sci. 358, 1663–1703.

Voight, B., Janda, R.J., Glicken, H., Douglass, P.M., 1983. Nature and mechanics of the Mount St Helens rockslide-avalanche of 18 May 1980. Geotechnique 33, 243–273. https://doi.org/10.1680/geot.1983.33.3.243.

Voight, B., Komorowski, J.C., Norton, G.E., Belousov, A.B., Belousova, M., Boudon, G., et al., 2002. The 26 December (Boxing Day) 1997 sector collapse and debris avalanche at Soufrière Hills Volcano, Montserrat. Geol. Soc. Mem. 21, 363–407. https://doi.org/10.1144/GSL.MEM.2002.021.01.17.